Identifying the key source rocks in heterogeneous saline lacustrine shales: Paleogene shales in the Dongpu depression, Bohai Bay Basin, eastern China

Tao Hu, Xiongqi Pang, Tianwu Xu, Changrong Li, Shu Jiang, Qifeng Wang, Yuanyuan Chen, Hongan Zhang, Chuang Huang, Shuangyi Gong, and Zhongchen Gao

ABSTRACT

Extensive, thick, and heterogeneous lacustrine shales occur globally with some regarded as source rocks, but which facies are the key contributors remains unclear. Previous studies have considered that all of the heterogeneous shales were source rocks in the Dongpu depression, but exploration does not support this assumption. Based on 40 yr of geochemical data collection, this study investigated the hydrocarbon generation and expulsion potential of these shales. The results show that laminated shales, though relatively limited in thickness and area, contain much higher organic matter contents and more oil-prone organic matter. Thermal simulation analysis shows that hydrocarbon generation and expulsion potential of laminated shales are much higher and more favorable for hydrocarbon expulsion. Oil-source correlation analyses between oil and shales indicate that northern oils feature pristane/phytane ratios (*Pr/Ph*) less than 0.7, gammacerane (gammacerane/C_{30}-hopane) indices greater than 0.5, and L-shaped distributions of ααα-C_{27}-20R, ααα-C_{28}-20R, and

Manuscript received May 4, 2018; provisional acceptance June 28, 2018; revised manuscript received August 14, 2018; revised manuscript provisional acceptance October 17, 2018; 2nd revised manuscript received April 30, 2020; 2nd revised manuscript provisional acceptance July 21, 2020; 3rd revised manuscript received September 3, 2020; 3rd revised manuscript provisional acceptance October 26, 2020; 4th revised manuscript received November 15, 2020; 4th revised manuscript provisional acceptance December 16, 2020; 5th revised manuscript received January 25, 2021; 5th revised manuscript provisional acceptance February 10, 2021; 6th revised manuscript received April 22, 2021; 6th revised manuscript provisional acceptance May 6, 2021; 7th revised manuscript received May 12, 2021; 7th revised manuscript provisional acceptance June 4, 2021; 8th revised manuscript received June 8, 2021; final acceptance June 17, 2021.
DOI:10.1306/01202218109

AUTHORS

TAO HU ~ *State Key Laboratory for Petroleum Resources and Prospecting, Beijing, China; Basin and Reservoir Research Center, College of Geosciences, China University of Petroleum (Beijing), Beijing, China; eric_hu_cup@126.com; thu@cup.edu.cn*

Tao Hu received his Ph.D. in geological resources and geological engineering from China University of Petroleum (Beijing) in 2018. He is now a lecturer of geological resources and geological engineering at China University of Petroleum (Beijing). His current research interests include petroleum resource assessment, petroleum accumulation mechanisms, and shale oil system evaluation. He is a corresponding author of this paper.

XIONGQI PANG ~ *State Key Laboratory for Petroleum Resources and Prospecting, Beijing, China; Basin and Reservoir Research Center, College of Geosciences, China University of Petroleum (Beijing), Beijing, China; pangxq@cup.edu.cn*

Pang Xiongqi received his Ph.D. in petroleum geology from China University of Geosciences (Beijing) in 1991. He is now a professor of geological resources and geological engineering at the China University of Petroleum (Beijing). His current research interests include basin analysis, petroleum resource assessment, and accumulation mechanisms. He is a corresponding author of this paper.

TIANWU XU ~ *Research Institute of Exploration and Development, Zhongyuan Oilfield Company, Sinopec, Zhengzhou, Henan, China; xutianwu@yahoo.com.cn*

Tianwu Xu received his Ph.D. in geological resources and geological engineering from China University of Petroleum (Beijing) in 2009. He is now a senior engineer at Zhongyuan Oilfield Company. His current research interest includes petroleum geology exploration. He is a corresponding author of this paper.

CHANGRONG LI ~ *State Key Laboratory of Petroleum Resources and Prospecting,*

Beijing, China; College of Geosciences, China University of Petroleum (Beijing), Beijing, China; li_changrong@qq.com

Changrong Li received his B.S. degree in resource exploration engineering from Northeast Petroleum University in 2018. In 2021, he graduated from China University of Petroleum (Beijing) with an M.S. degree. His research interests include petroleum resource assessment (methods and applications), petroleum systems, and basin analysis.

SHU JIANG ~ *Key Laboratory of Tectonics and Petroleum Resources of Ministry of Education, China University of Geosciences, Wuhan, Hubei, China; Jiangsu@cug.edu.cn*

Shu Jiang received his Ph.D. in petroleum geology from China University of Geosciences (Wuhan) in 2005. He is now a chair professor of petroleum engineering at the China University of Geosciences (Wuhan). His current research interests include basin analysis and unconventional hydrocarbon resources.

QIFENG WANG ~ *Research Institute of Petroleum Exploration and Development, PetroChina, Beijing, China; wqf2020@petrochina.com.cn*

Qifeng Wang received her Ph.D. in geology from China University of Petroleum (Beijing) in 2020. She is now an engineer of gas field development at Research Institute of Petroleum Exploration and Development, PetroChina. Her current research interests include petroleum resource assessment and reservoir geological modeling.

YUANYUAN CHEN ~ *State Key Laboratory for Petroleum Resources and Prospecting, Beijing, China; Basin and Reservoir Research Center, College of Geosciences, China University of Petroleum (Beijing), Beijing, China; 805650259@qq.com*

Yuanyuan Chen received her B.S. degree in resource exploration engineering from China University of Petroleum (Beijing) in 2018. She is now a graduate student majoring in geological resources and geological engineering at the China University of Petroleum (Beijing). Her current research interests include organic matter accumulation mechanism and basin analysis.

$\alpha\alpha\alpha$-C_{29}-20R regular steranes, and are similar to the biomarker characteristics of northern laminated shales with total organic carbon (*TOC*) contents greater than 1 wt. %. In contrast, northern massive shales are characterized by a high *Pr/Ph* and low gammacerane index. Southern oils feature *Pr/Ph* greater than 0.7, gammacerane indices less than 0.5, and L-shaped distributions of regular steranes that are similar to the biomarker characteristics of southern laminated shales. Southern massive shales were characterized by high *Pr/Ph*, low gammacerane indices, and reversed L- and V-shaped distributions. Laminated shales with *TOC* contents greater than 1 wt. % are the key source rocks in these heterogeneous Paleogene shales.

INTRODUCTION

Heterogeneous lacustrine shales developed widely across the globe, and include the Green River Formation in Uinta Basin, United States (Katz, 1995); the Lower Cretaceous of the Brazilian marginal basins (Mello et al., 1991); the Oligocene shales in the Assam Basin, India (Saikia and Dutta, 1980); the Brown Shale of Indonesia (Katz and Kahle, 1988); and the Qingshankou Formation in the Songliao Basin, northeastern China (Halbouty, 1980; Wang et al., 2019). Over the past 40 yr of global petroleum exploration, one of the most striking achievements has been the discovery of extensive and thick shales in lacustrine basins, with a cumulative thickness of 100 to 800 m or even 2000 to 3000 m (Jin, 2001; Zhu and Jin, 2003), such as the Paleogene shales offshore (Jiang et al., 2016), in the Dongpu depression (DD) (Hu et al., 2018a, 2021), Bonan sag (Wang et al., 2015b), and the Dongying depression (Chen et al., 2016) in the Bohai Bay Basin; the Paleogene shales in the Pearl River Mouth Basin (Jiang et al., 2015; Cao et al., 2018); the Triassic shales in the Ordos Basin (Li et al., 2020); and the Permian shales in the Junggar Basin (Hu et al., 2018b). The total organic carbon (*TOC*) content of these lacustrine shales is highly variable (0.1–25 wt. %) and generally less than 4 wt. % (Wang et al., 2019). Furthermore, the average *TOC* content of the shales in the Fengcheng area of the Junggar Basin and the DD of the Bohai Bay Basin (Zou et al., 2019) is approximately 1 wt. %. Especially in the DD, the percentage of shales with *TOC* < 1 wt. % approaches 80% among the 6328 analyzed Paleogene shale samples (Zhang et al., 2017). Generally, lacustrine shales are characterized by strong heterogeneity, consisting of a highly variable organic matter composition and organic matter and mineral contents, occurring in various organic facies (Wicks et al., 1991; Katz, 1995; Peters et al., 2008; Wang et al., 2019). However, previous studies largely considered the whole set of lacustrine shales as source rocks regardless of the organic facies (Zhu and Jin, 2003; Deng and Sun, 2019). A key question

remains, are all extensive and extremely thick lacustrine shales effective source rocks?

Many studies have been performed to address this issue. Initially, researchers proposed some *T*OC criteria for source rock evaluation (Peters and Cassa, 1994; Huang and Xin, 1995). With the development of petroleum geochemistry techniques, it was recognized that the hydrocarbon expulsion process and efficiency were more important than the single *T*OC parameter (Momper, 1978; Pang et al., 2005). Momper (1978) suggested that in most cases, hydrocarbon expulsion cannot occur until a threshold amount of bitumen had been generated in source rocks and proposed the threshold amount was approximately 50 million barrels per cubic mile. Lewan and Williams (1987) investigated petroleum generation from resinite through hydrous pyrolysis and evaluated the hydrocarbon expulsion of source rocks. Pang et al. (1993) and Pang (1995) stated that only shales where hydrocarbon expulsion occurred could be regarded as source rocks and further proposed a hydrocarbon expulsion threshold, which indicates that hydrocarbon expulsion occurs only when shales are saturated with hydrocarbons in different forms: adsorbed, free, oil-soluble, and water-soluble hydrocarbons. Liang (1998) evaluated the thick shales in the Manjiaer depression, Tarim Basin, and found that the shales distributed in the slope area are the key source rocks, which featured a high *T*OC content but were limited in thickness to only tens of meters. By investigating the hydrocarbon expulsion process of the Paleogene shales in the Dongying depression, Jin et al. (2001) held that the source rocks could generate significant volumes of hydrocarbons even with only tens of meters in thickness. After that, Zhu and Jin (2003) found that the thin shales of only tens of meters in thickness are the effective source rocks in the Dongying depression, instead of the whole set of Paleogene shales (500–800 m). Based on mass balance theory, Pang et al. (2005) proposed the hydrocarbon generation potential method and evaluated the hydrocarbon expulsion quantity of the Eocene-Oligocene shales in the Niuzhuang South Slope, Bohai Bay Basin, and finally identified the key source rocks. Based on the hydrocarbon generation potential method, Jiang et al. (2015, 2016), Hu et al. (2016), and Peng et al. (2016) simulated the hydrocarbon expulsion quantity of the lacustrine shales in the South China Sea, Junggar Basin, and Bohai Sea area and identified the actual source rocks within the extensive and thick shales. However, many studies still assessed the gross lacustrine shale section, even the shales with dispersed organic matter (Hakimi et al., 2012; Jiang et al., 2016; Tian et al., 2017).

This problem also occurs in marine petroleum systems. For nearly 30 yr, the Triassic marine carbonate Shublik Formation was confirmed as a key source rock in the North Slope of Alaska, accounting for one-third of the oil in the supergiant Prudhoe Bay

HONGAN ZHANG ~ *Zhongyuan Oilfield Company, Sinopec, Puyang, Henan, China; zhangha.zyyt@sinopec.com*

Hongan Zhang received his Ph.D. in petroleum geology from China University of Geosciences (Beijing) in 2004. He is now a professor engineer and vice president at Zhongyuan Oilfield Company. His current research interest includes petroleum geology exploration.

CHUANG HUANG ~ *Research Institute of Exploration and Development, Yanchang Oilfield Company, Yanan, Shanxi, China; 363583422@qq.com*

Chuang Huang received his M.S. degree in geological engineering from China University of Petroleum (Beijing) in 2019. He is now a geological engineer with Yanchang Oilfield Company. His current research interest includes reservoir geological modeling.

SHUANGYI GONG ~ *State Key Laboratory for Petroleum Resources and Prospecting, Beijing, China; Basin and Reservoir Research Center, College of Geosciences, China University of Petroleum (Beijing), Beijing, China; Shuangyi.gong@outlook.com*

Shuangyi Gong received her B.S. degree in geological engineering in 2017 and M.S. degree in geological resources and geological engineering in 2020 from China University of Petroleum (Beijing). Now she is pursuing her Ph.D. at the University of Manchester, United Kingdom.

ZHONGCHEN GAO ~ *Petroleum Exploration and Production Research Institute, Jianghan Oilfield, Wuhan, Hubei, China; gaozhch88.jhyt@sinopec.com*

Zhongchen Gao received his M.S. degree in geological engineering from China University of Petroleum (East China) in 2014. He is now a geological engineer at Petroleum Exploration and Production Research Institute, Jianghan Oilfield. His current research interests include hydrocarbon accumulation mechanisms and reservoir geological modeling.

ACKNOWLEDGMENTS

This study was financially supported by the China Postdoctoral Science Foundation (2019M660054), Science Foundation of China University of Petroleum (Beijing) (2462019BJRC005), National Natural Science Foundation of China (41872148), 2017 AAPG Foundation Grants-in-Aid Program (15388), National Basic Research Program of China (2011CB2011-02), and the Science Projects of the Sinopec Zhongyuan Oilfield Company (P15022).

field and nearly all the oil in the second-largest Kuparuk River field (Magoon and Bird, 1985; Bird, 1994; Peters et al., 2006). Recent studies conducted by Peters et al. (2006), Wang et al. (2014), and Yurchenko et al. (2018) indicated that the oil was linked to the calcareous and shaly organofacies of the Shublik source rocks. Therefore, in regard to the extensive and extremely thick lacustrine shales, it remains unclear whether both high– and low–organic-matter-content shales contribute to petroleum pools, or which shale organofacies are key contributors. This should be the foremost aim in petroleum resource evaluation in lacustrine basins.

The DD is a typical lacustrine basin in China, in which extensive and extremely thick Paleogene shales occur (Wang et al., 2015a; Zhang et al., 2017). Over 40 yr of petroleum exploration, more than 20,000 wells were drilled and abundant geochemical data accumulated. Based on a preexisting rich data set and test data on 65 newly collected shale samples, 90 oil samples, and 3 sandstone samples, this study analyzed the lithology, organic matter content, organic matter precursors, and thermal maturity. Thermal simulation experiments were performed to compare the hydrocarbon generation and expulsion characteristics of the Paleogene shales with different lithofacies (forward analysis). Biomarker-based oil-source correlations were conducted to trace the petroleum source and confirm the key source rocks (inverse analysis). By combining the forward and inverse analysis, key source rocks would be identified among the extensive and extremely thick lacustrine shales.

GEOLOGICAL SETTING

The DD is a Cenozoic lacustrine depression in the Linqing subbasin, Bohai Bay Basin, with an area of 5300 km^2 (Figure 1). The DD is narrow in the north and broad in the south, and it is bounded by the Luxi uplift to the east, the Neihuang uplift to the west, the Lankao uplift to the south, and the Shenxian uplift to the north. Its structures are generally controlled by faults, including the western slope, western sag, central uplift, eastern sag, and eastern steep slope zones (Figure 2) (Wang et al., 2015a). Two tectonic phases occurred during the Cenozoic: the Paleogene-Neogene rift subsidence stage and the late Quaternary sag. Between these two tectonic phases, regional uplift occurred, and a regional unconformity was formed (Su et al., 2006). The Paleogene strata include the Kongdian, Shahejie (E_2s), and Dongying (E_3d) Formations (Figure 3). Lake level frequently changed during Paleogene E_2s sedimentation. Four members were developed in the E_2s. The upper submember of the fourth member ($E_2s_4^U$) Formation was deposited in lakeshore-fluvial facies, while the third member (E_2s_3) was developed in deep and semideep lake

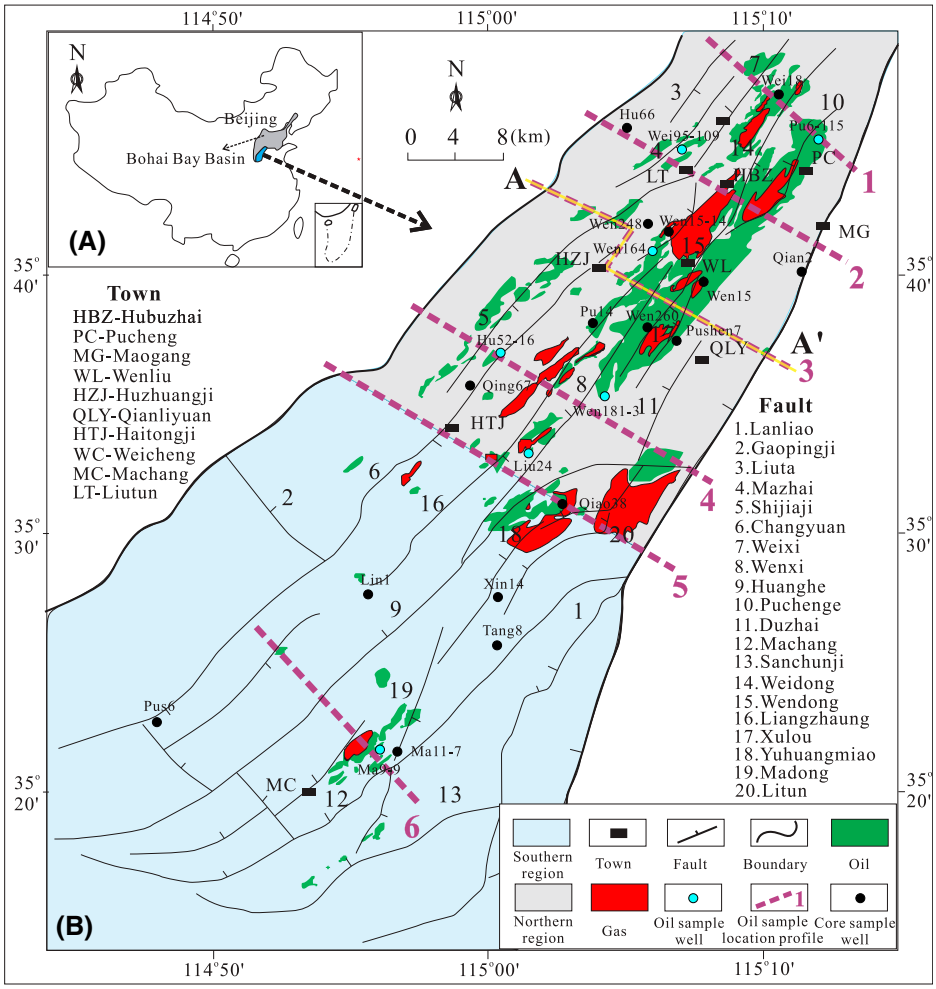

Figure 1. (A) Overview map of China showing the location of Bohai Bay Basin and Dongpu depression (DD). (B) Distribution of faults (middle of the third member of Shahejie Formation) and fields in the DD, modified after Wang et al. (2015a).

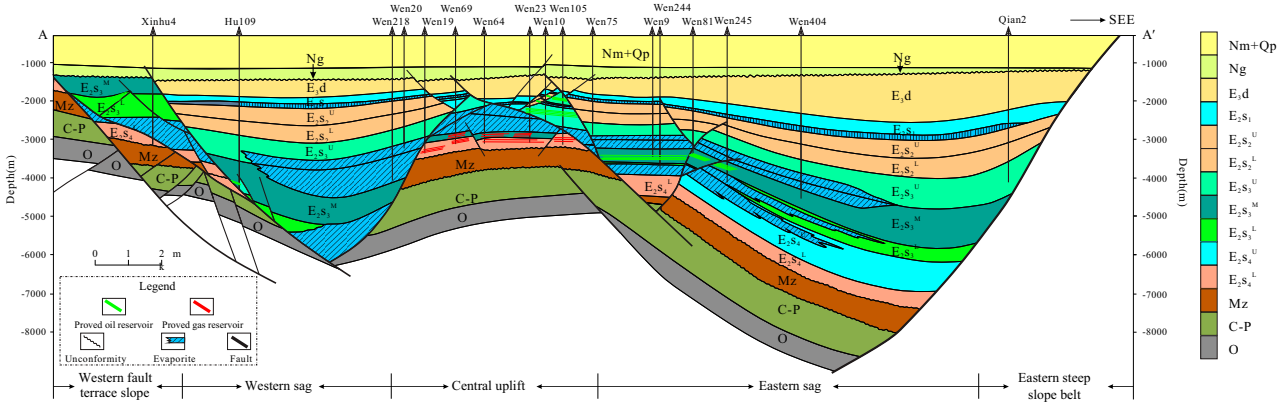

Figure 2. Representative cross section (AA′) showing the basic geological framework, modified after Wang et al. (2015a). C = Carboniferous; E_2s = Shahejie Formation; $E_2s_1^L$ = lower submember of first member of E_2s; $E_2s_1^U$ = upper submember of first member of E_2s; $E_2s_2^L$ = lower submember of second member of E_2s; $E_2s_2^U$ = upper submember of second member of E_2s; $E_2s_3^L$ = lower submember of third member of E_2s; $E_2s_3^M$ = middle submember of third member of E_2s; $E_2s_3^U$ = upper submember of third member of E_2s; $E_2s_4^L$ = lower submember of fourth member of E_2s; $E_2s_4^U$ = upper submember of fourth member of E_2s; E_3d = Dongying Formation; Mz = Mesozoic; Ng = Guantao Formation; Nm = Minghuazhen Formation; O = Ordovician; P = Permian; Qp = Pingyuan Formation.

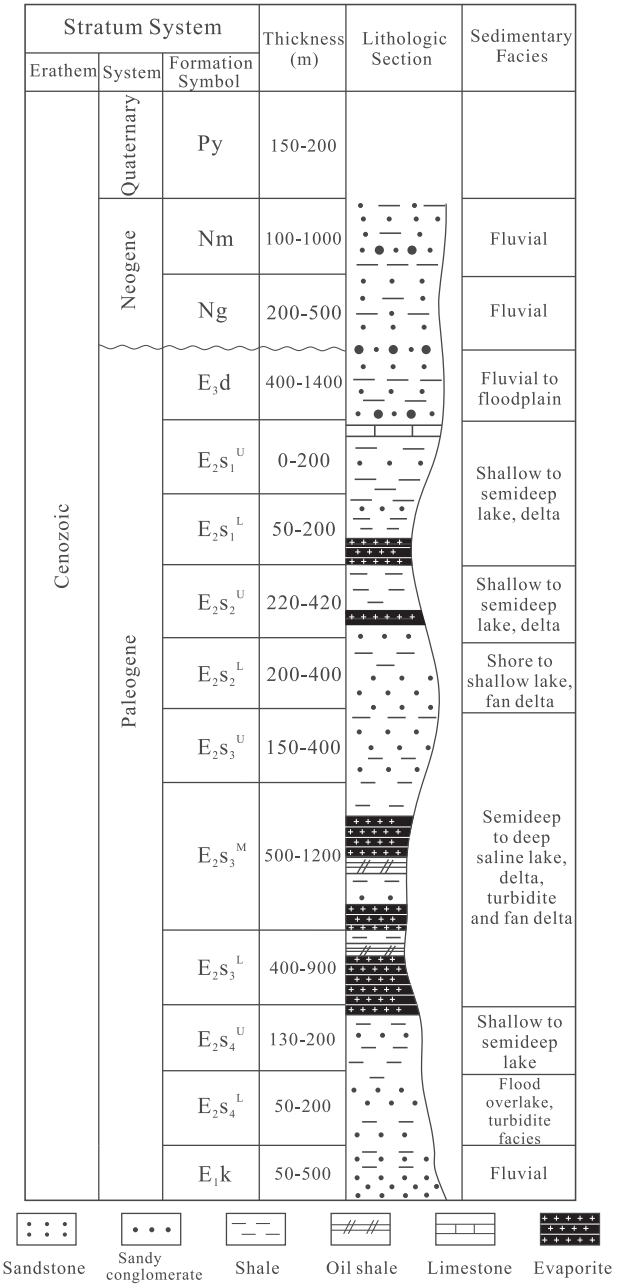

Figure 3. Generalized Paleogene stratigraphy of the Dongpu depression. E_1k = Kongdian Formation; E_2s = Shahejie Formation; $E_2s_1^L$ = lower submember of first member of E_2s; $E_2s_1^U$ = upper submember of first member of E_2s; $E_2s_2^L$ = lower submember of second member of E_2s; $E_2s_2^U$ = upper submember of second member of E_2s; $E_2s_3^L$ = lower submember of third member of E_2s_3; $E_2s_3^M$ = middle submember of third member of E_2s_3; $E_2s_3^U$ = upper submember of third member of E_2s; $E_2s_4^U$ = upper submember of fourth member of E_2s; $E_2s_4^L$ = lower submember of fourth member of E_2s; E_3d = Dongying Formation; Ng = Guantao Formation; Nm = Minghuazhen Formation; Qp = Pingyuan Formation.

facies, with extensive and thick shales having been deposited. The second member of E_2s (E_2s_2) mainly consisted of lakeshore-fluvial facies deposits. Both lower submember of first member ($E_2s_1^L$) and upper submember of first member ($E_2s_1^U$) Formations were developed in semideep lake and delta facies, respectively (Ji and Feng, 2003). The shales in the northern region were vertically interbedded with four sets of evaporites (Wang et al., 2015a). The Paleogene shales were mainly developed in $E_2s_4^U$, E_2s_3, and $E_2s_1^L$ (Wu et al., 2003), and the former two formations are predominant (Zhang et al., 2017). Paleogene shales are widespread throughout the DD and are mainly distributed in the Pucheng-Qianliyuan, Liutun-Haitonji, Gegangji, Nanhejia-Menggangji, and Guancheng sags. The cumulative thickness of the shales is great, with an average thickness ranging from 500 to 1026 m in the different sags, with the greatest thickness reaching 2750 m (Wu et al., 2003; Duan et al., 2008; Hu et al., 2021).

SAMPLES AND METHODS

Samples

Based on the preexisting 40-yr geochemical data set and an additional 65 shale samples of different lithofacies, 90 oil samples and 3 siltstone samples from northern well Wei 18-5 and the southern Machang area were collected. The sampled wells are shown in Figure 1B.

Methods

To prepare for the *TOC* measurement, the shale samples were first crushed to 200-mesh and then treated with a 10% hydrochloric acid solution at 60°C to remove carbonate minerals. The samples were then washed with distilled water to remove any remaining acid before being dried at 50°C. Finally, *TOC* content was measured with a LECO CS-400 analyzer. A Rock-Eval II instrument was used for the pyrolysis measurements. Vitrinite reflectance (R_o) was measured using a Zeiss microscope equipped with a CRAIC microscope photometer instrument (Taylor et al., 1998). Before the measurement, the

instrument was calibrated with the yttrium-aluminum-garnet reflectance standard (0.9%). The measurements were conducted with an oil-immersion lens under reflected light at a wavelength of 546 nm with a 40× oil-immersion objective (1.518 refractive index oil).

For gas chromatography (GC) and GC-mass spectrometry (GC-MS) analyses, 72-hr Soxhlet extraction was performed on the shale samples. Then, the saturated hydrocarbon samples were separated from both the shale extracts and oil using open silica gel column chromatography. The GC analysis was conducted with an HP 6890 chromatograph (30 m × 0.32 mm) with nitrogen as the carrier gas. Each sample was first maintained at 80°C for 5 min, then heated to 290°C at a rate of 4°C/min and held at 290°C for 30 min. The GC-MS analysis was performed with an Agilent 5973I instrument equipped with an HP 6890 chromatograph (30 m × 0.32 mm) with helium as the carrier gas. Each sample was initially kept at 60°C for 5 min, heated to 120°C at a rate of 8°C/min, heated to 290°C at a rate of 2°C/min, and maintained at 290°C for 30 min.

A biological microscope with fluorescence emission was used to observe kerogen macerals. Transmission light thin slices of kerogen were prepared using either glycerol or polyethylene. During measurement, kerogen thin slices were first observed via a 40× object lens to determine the representative maceral size. This size was regarded as the standard statistical unit. The visual field of the microscope was moved at constant distance intervals, and the center of each visual field was selected as the fixed maceral coordinate. Then, the macerals observed in the visual field were identified and counted. Field emission scanning electron microscopy (FE-SEM) images were obtained with an FEI Quanta model 200 F instrument at an operating voltage of 20 kV and distance of 10 mm. During the experiment, argon ion polishing was first performed on the shale samples to attain a nanoscale surface flatness; a finely focused electron beam was then scanned across the surface, and backscattered scanning electron signals of the surface were collected to image morphology (Loucks et al., 2009).

Hydrocarbon generation simulation experiments were conducted with a DK-II instrument. Due to the heterogeneity of lacustrine shales, the shale samples were crushed into 60-mesh particles. A total of 50 to 150 g of the crushed samples was then loaded into a chamber with a diameter of 3.5 cm and a height of 10 cm and then compressed under a lithostatic pressure of approximately 5 MPa to obtain cylindrical samples. The pore spaces in the cylindrical samples and the remaining spaces in the reaction vessel were then completely filled with water under pressure. The heating rate was 1°C/min, and the preset temperature ranged from 250°C to 550°C. The followed procedures are described in Zheng et al. (2009).

RESULTS

Lithology and Organic Matter Content

Lamina refers to the single layers with a thickness of less than 1 mm (Lazar et al., 2015; Liu et al., 2018b). Depending on whether laminations develop, shales can be divided into two categories: laminated and massive shales (Calvert et al., 1996; Liu et al., 2018a). In the DD, the Paleogene shales mainly consist of massive shales (Figure 4A–C), representing nearly 80% of the section. Laminated shales feature a high degree of lamination (Figure 4D–F). In detail, laminated shales are characterized by two types of layers, including organic-rich lamina and calcareous lamina containing pyrite (Figure 4E), similar to the laminated texture of the shales in the Dongying depression (Chen et al., 2016). When hydrochloric acid is applied to laminated shales, many colorless tiny bubbles are first formed on the surface of the calcareous lamina. Then, the colorless hydrochloric acid solution gradually turns light green with the gradual disappearance of the bubbles because Fe^{2+} is generated from the chemical reaction between the pyrite in the calcareous lamina and hydrochloric acid ($FeS_2 + 2HCl = FeCl_2 + H_2S\uparrow + S\downarrow$) (Figure 4F). Moreover, the fresh fracture surfaces of laminated shales exhibit a greasy luster. The organic-rich lamina burn, emitting black smoke with a distinct gasoline odor.

Microscopic observation of the laminated shales from wells Wei 79-13 and Wen 200-6 reveals many organic-rich lamina with a continuous and bright yellow fluorescence, whose texture and morphology are very clear, and the thickness of each organic-rich lamina ranges from 10 to 50 μm (Figure 5A–C). These laminae might be sourced from densely layered alginite (Zhang et al., 2017). In comparison, the massive shales mainly contain dispersed organic matter, with

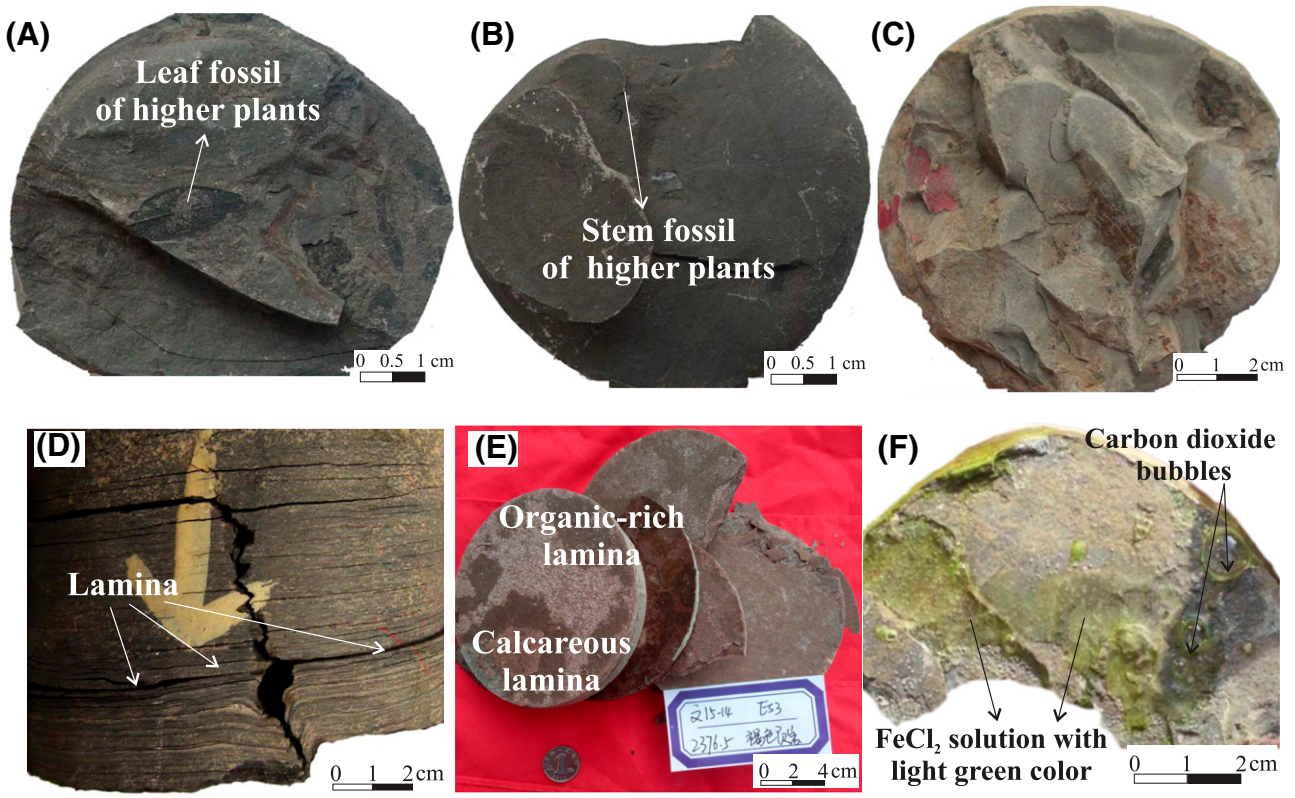

Figure 4. Core photos of Shahejie shales. (A) Well Qian 2, upper submember of third member of Shahejie Formation ($E_2s_3^U$), ~3801.3–3803.35 m, massive shale, *TOC* = 0.42 wt. %; (B) well Qian 2, $E_2s_3^U$, 3775 m, massive shale, *TOC* = 0.40 wt. %; (C) well Hu 66, middle submember of third member of E_2s ($E_2s_3^M$), 1776 m, massive shale; (D) well Pushen 7, $E_2s_3^M$, ~3561.40–3561.50 m, laminated shale; (E) well Wen 15-14, E_2s_3, 2376.5 m, laminated shale, *TOC* = 2.58 wt. %; (F) well Wen 15-14, E_2s_3, 2378.2 m, laminated shale. *TOC* = total organic carbon.

elliptical and irregular shapes and yellow fluorescence (Figure 5D–F), which are likely sourced from dispersed telalginite (Zhang et al., 2017; Liu et al., 2018b).

The 40-yr geochemical data set shows that the *TOC* content of the northern shales ranges from 0.01 to 11.54 wt. %, with a mean of 0.81 wt. %, and the *TOC* content of the southern shales ranges from 0.04 to 4.12 wt. %, with a mean of 0.41 wt. %, implying that the organic matter content of the northern shales is generally higher than that of the southern shales, but the mean values are both lower than 1 wt. % (Figure 6). Combined with the sedimentary facies, burial depth, and measured *TOC* data, the *TOC* isolines of the shales in E_2s Formation were constructed (Figure 7), verifying that the organic matter content of the northern shales is generally greater than that of the southern shales.

According to the evaluation criterion proposed by Peters and Cassa (1994), the contents of 18.1%, 6.4%, and 1.4% of the northern shales are good (1 wt. % < *TOC* < 2 wt. %), very good (2 wt. % < *TOC* < 4 wt. %), and excellent (*TOC* > 4 wt. %), respectively, and the corresponding ratios of the southern shales are 5.1 wt. %, 1.7 wt. %, and 0.1 wt. %, respectively (Figure 6), showing that few shales with good–excellent organic matter contents are developed in the DD, which is consistent with previous studies (Wang et al., 2015a; Zhang et al., 2017). In comparison, the scale of the shales with good–excellent organic matter contents in the northern region is greater than that of the southern region.

To investigate the *TOC* variation in the shales with different lithofacies in the vertical direction, continuous core sampling was conducted in wells Wen 248 and Wen 260. The results show that the *TOC* content changed dramatically across tens of centimeters, and the *TOC* content of the laminated shale intervals is generally greater than that of the massive shale intervals. The thickness of laminated shales accounts for 5%–15% of the total stratigraphic thickness (Figure 8).

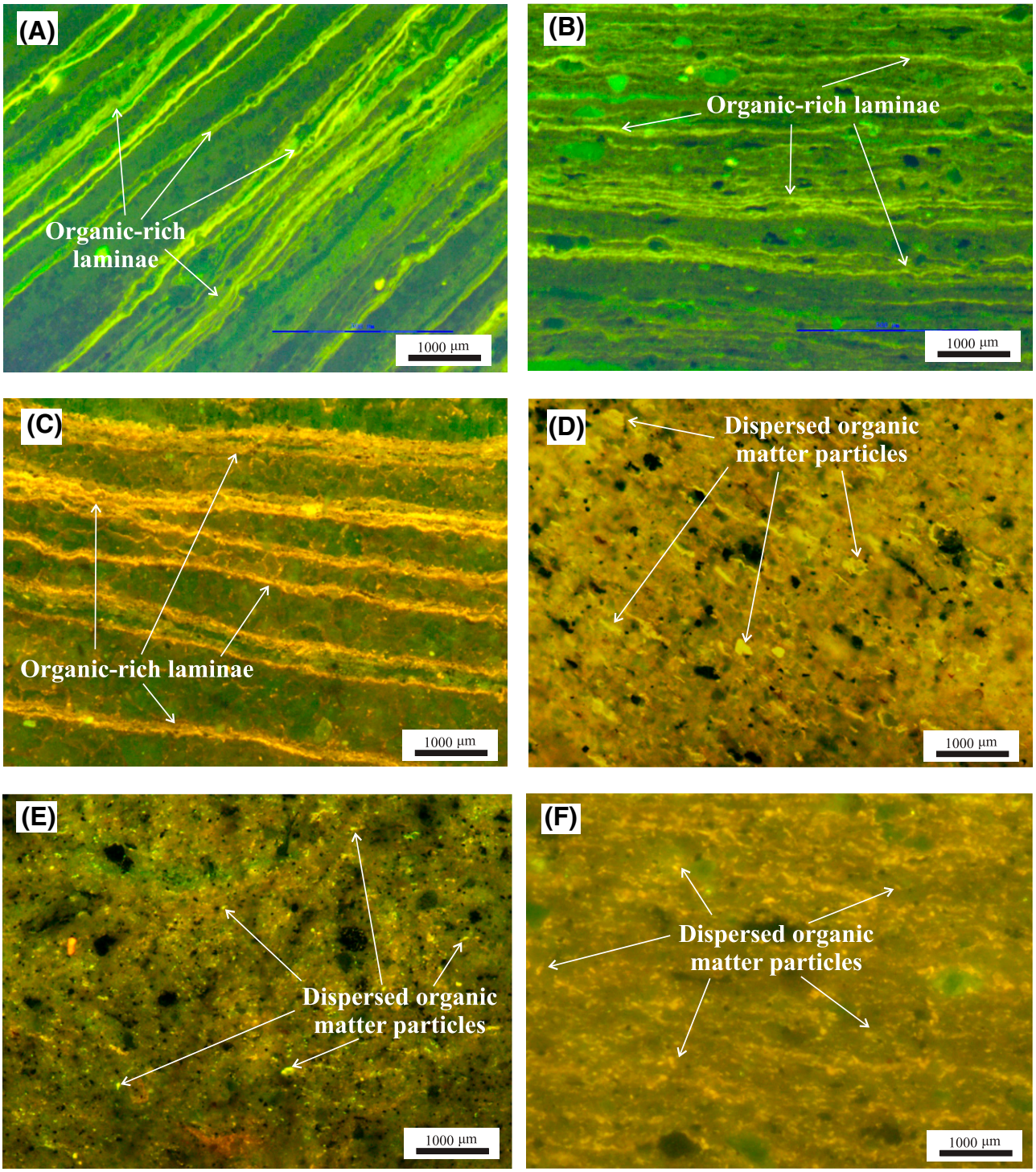

Figure 5. Fluorescent images showing the textures within the Shahejie shales. (A) Well Wei 79-13, middle submember of third member of Shahejie Formation ($E_2s_3^M$), 3362 m, laminated shale, total organic carbon (*TOC*) = 5.35 wt. %, ×200; (B) well Wei 79-13, $E_2s_3^M$, 3374.78 m, laminated shale, *TOC* = 2.24 wt. %, ×200; (C) well Wen 200-6, lower submember of first member of E_2s ($E_2s_1^L$), 3298.8 m, laminated shale, *TOC* = 2.08 wt. %, ×200; (D) well Pu 131, $E_2s_1^L$, 2418.57 m, massive shale, *TOC* = 2.23 wt. %, ×400; (E) well Wei 63, E_2s_1, 1767.86 m, massive shale, *TOC* = 1.46 wt. %, ×200; (F) well Wen 200-6, $E_2s_1^L$, 3294.14 m, massive shale, *TOC* = 3.56 wt. %, ×400.

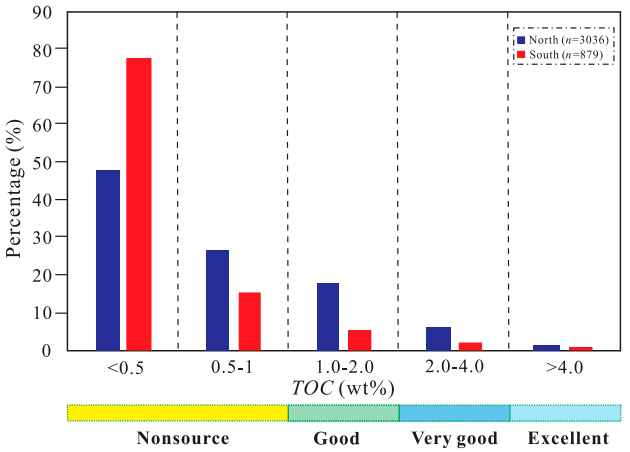

Figure 6. Frequency histograms of total organic carbon (*TOC*) contents of the Shahejie shales. The evaluation standard is from Peters and Cassa (1994). *n* = number of samples.

The *T*OC and hydrocarbon generation potential (pyrolysis *PG* [S_1 + S_2]) of the Shahejie shales are shown in Figure 9 and Table 1. In the northern region, the laminated shales account for 53% and 92% of the very good–excellent (*T*OC > 2 wt. %, *PG* > 12 mg/g) organic matter contents, respectively, and in the southern region, they account for 71% of the very good–excellent organic matter contents, showing that most of the high-quality source rocks are laminated shales.

Organic Petrographic Characteristics

Optical microscopy, FE-SEM, and energy spectrum experiments were employed to investigate the morphology (shape and size) and fluorescence of the organic matter precursors in the shales (Figure 10). The results show that the laminated shales in the northern and southern regions are both mainly composed of sapropelinites and exinite (Figure 11). Sapropelinites are mainly translucent, heterogeneous, flocculent, or hydrogen-rich amorphous material with an average content of approximately 60% (the maximum content is 96%), exhibiting a yellowish-brown color under transmitted light. The particle size ranges from tens to hundreds of micrometers (Figures 5; 10A, B). Sapropelinites, such as alginite, mainly originate from lower aquatic organisms and have a high hydrocarbon generation potential. Alginite is the degradation product of algae, some of which contain distinct degradation traces (Figure 10C, D) or is well preserved with elliptic (Figure 10E–I) and cylindrical shapes (Figure 10J). Further observation shows that most of the algae are dinoflagellate cysts (Figure 10K), spiny dinoflagellates (Figure 10L–N), *Aegagropila linnaei* (Figure 10O), and *Chytroeisphaeridia* (Figure 10P). In comparison, the alginite content is much lower than the hydrogen-rich amorphous content. This mainly occurs due to the low resistance to degradation of algae, most of which has been converted into hydrogen-rich amorphous matter rather than alginite (Burgess, 1974; Rahman and Kinghorn, 1995). The kerogen within the massive shales is mainly composed of vitrinite (Figure 11), which is derived mainly from terrestrial higher plants (Figures 4A–C, 10Q–T).

Thermal Maturity

The results show that the Paleogene shales are generally in the peak mature and late mature stages, with shales within the postmature stage mainly distributed in the Qianliyuan and Huqin regions (Figure 12).

Thermal Simulation Characteristics

Because laminated and massive shales are mainly developed in the DD, and obvious differences exist in organic matter contents and types between them, one laminated and one massive immature core sample with similar *T*OC were selected to compare the hydrocarbon generation potential by conducting a thermal simulation experiment. The sample information is shown in Figure 13. The results show that for the laminated shale, with increasing simulation temperature, the residue, oil generation, oil expulsion, and hydrocarbon generation rates first increased and then decreased, reaching peak values of 560, 655, 383, and 760 kg per ton organic carbon (kg/tc), respectively, at temperatures of 327°C, 338°C, 427°C, and 550°C, respectively. The gas generation rate increases with increasing simulation temperature, reaching a peak value of 398 kg/tc at 550°C (Figure 13A). For the massive shale, with increasing simulation temperature, the residue, hydrocarbon generation, oil generation, and oil expulsion rates first increased and then decreased, reaching peak values of 329, 431, 380, and 171 kg/tc, respectively, at temperatures of 350°C, 359°C, 362°C, and 420°C, respectively. The gas generation rate increased with

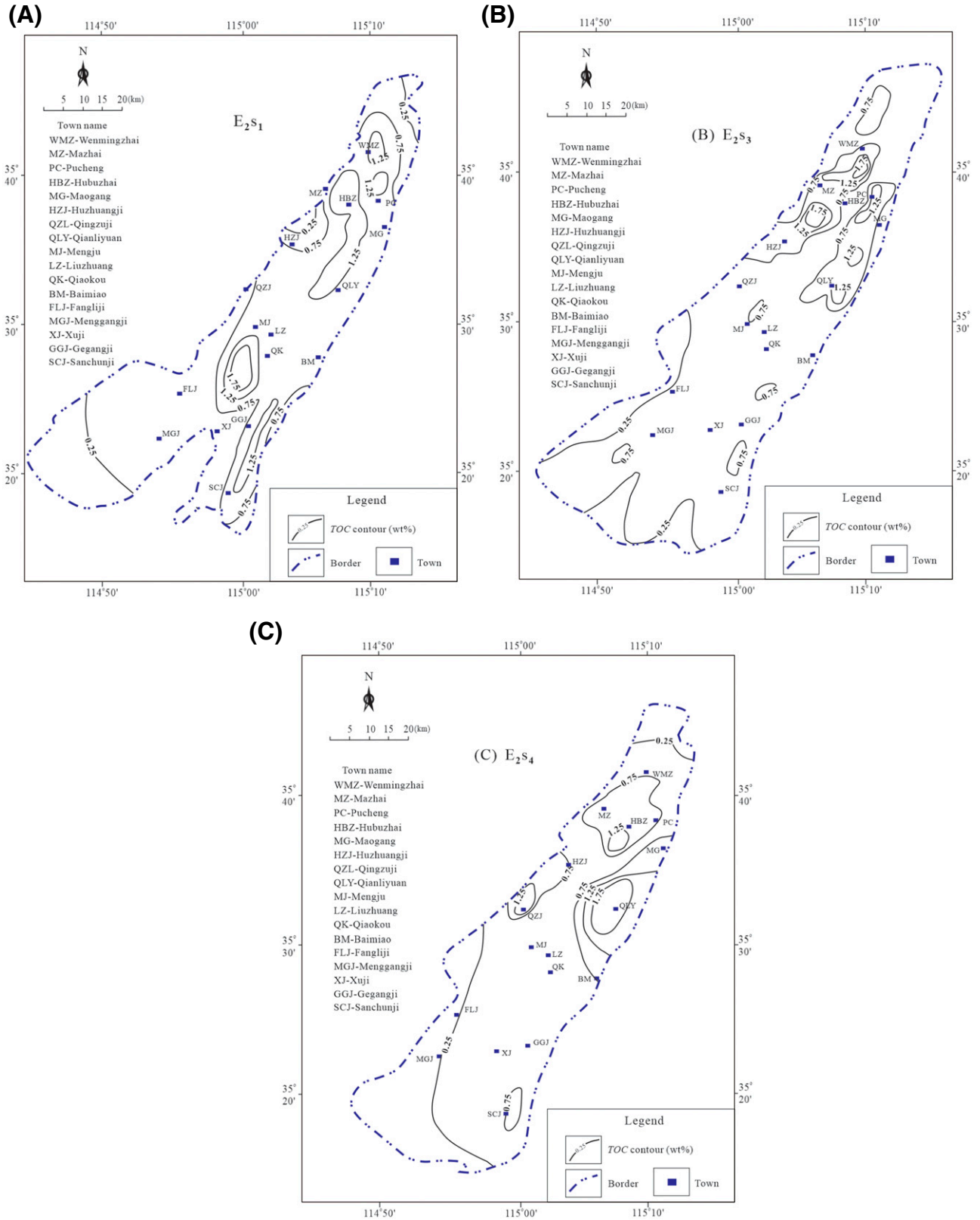

Figure 7. Average total organic carbon (*TOC*) contour maps of the main shale intervals in the Shahejie Formation (E_2s). (A) First member of E_2s (E_2s_1). (B) Third member of E_2s (E_2s_3). (C) Fourth member of E_2s (E_2s_4).

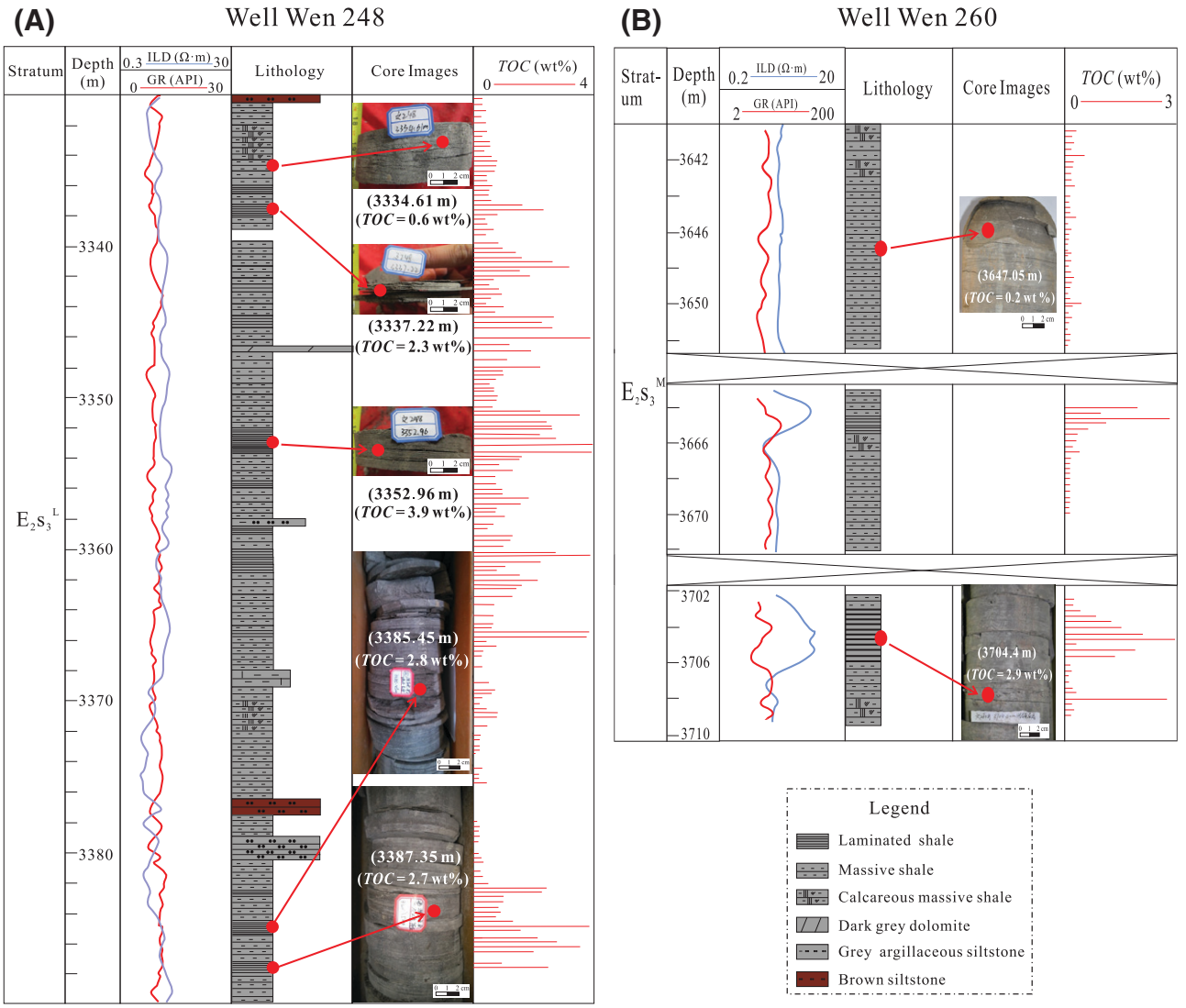

Figure 8. Vertical total organic carbon (*TOC*) content variation with different lithofacies in typical wells. (A) Well Wen 248; (B) well Wen 260. $E_2s_3^L$ = lower submember of third member of Shahejie Formation; $E_2s_3^M$ = middle submember of third member of E_2s; GR = gamma ray; ILD = deep resistivity.

increasing simulation temperature, reaching a peak value of 177 kg/tc at 500°C (Figure 13B).

Biomarker Characteristics

Shale Core Samples

The results show that the northern laminated shales feature low pristane (*Pr*) and high phytane (*Ph*) and gammacerane contents and L-shaped C_{27}, C_{28}, and C_{29} distributions (Figures 14A–C and 15D–I, respectively). The *Pr*/*Ph* and gammacerane indices of the northern laminated shales range from 0.25 to 0.59 (average of 0.38) and from 0.31 to 4.03 (average of 1.34), respectively (Table 2). In comparison, the northern massive shales feature high *Pr* and low *Ph* and gammacerane contents and reversed L-, V-, or L-shaped C_{27}, C_{28}, and C_{29} distributions (Figures 14E–G and 15P–R, respectively). The *Pr*/*Ph* and gammacerane indices of the northern massive shales range from 0.21 to 0.94 (average of 0.55) and from 0.10 to 2.10 (average of 0.54), respectively (Table 2). In the southern region, the laminated and massive shale are both characterized by high *Pr* and low *Ph* and gammacerane contents (Figure 16J–U), and the *Pr*/*Ph* and gammacerane indices range from 0.4 to 1.76 (average of 0.84) and from 0.15 to 0.51 (average of 0.32), respectively (Table 2). The distribution of C_{27}, C_{28}, and C_{29} steranes in the southern laminated shales exhibit an L shape, with the highest

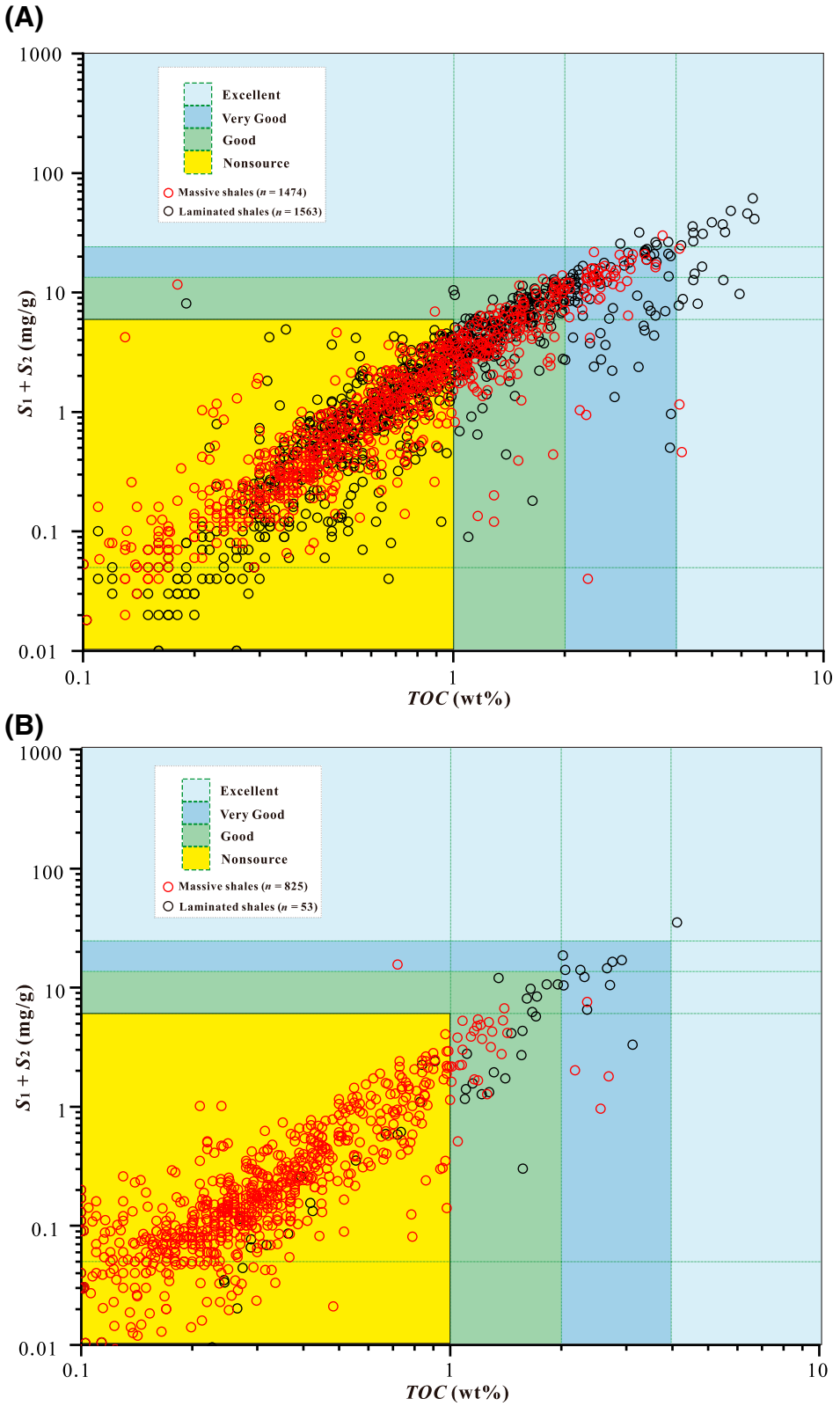

Figure 9. Correlation between total organic carbon (*TOC*) and hydrocarbon generation potential, which is the sum of residual hydrocarbons and pyrolysis hydrocarbons ($S_1 + S_2$) of the Shahejie shales. (A) Northern region; (B) southern region. The evaluation standard is from Peters and Cassa (1994).

Table 1. Total Organic Carbon and Potential Hydrocarbon Generation Values of Shahejie Shales in the Dongpu Depression, Bohai Bay Basin

Region	Lithology	*TOC* (wt. %)	*PG* (mg/g)
Northern	Laminated shale	0.01–11.54 (avg 0.87)	0.01–72.93 (avg 3.05)
Northern	Massive shale	0.04–4.52 (avg 0.74)	0.01–33.40 (avg 2.19)
Southern	Laminated shale	0.19–4.12 (avg 1.32)	0.01–35.18 (avg 5.24)
Southern	Massive shale	0.04–2.69 (avg 0.35)	0.01–15.63 (avg 0.42)

Abbreviations: avg = average; *PG* = hydrocarbon generation potential; *TOC* = total organic carbon.

content for C_{27} and the lowest content for C_{28} (Figures 14D; 16R, U), but the distribution in the southern massive shales exhibits reversed L or V shapes (Figures 14H; 16L, O, respectively).

Oil Samples

The results of the 90 oil samples reveal that the northern oil samples (profiles 1, 2, 3, 4, and 5 in Figure 1B) are characterized by low *Pr* and high *Ph* and gammacerane contents and an L-shaped distribution of C_{27}, C_{28}, and C_{29} steranes (Figure 15A–C and J–O, respectively). The *Pr*/*Ph* and gammacerane indices of the northern oil samples range from 0.16 to 0.87 (average of 0.51) and from 0.37 to 2.63 (average of 0.83), respectively (Table 3). In comparison, the southern oil samples (profile 6 in Figure 1B) feature high *Pr* and low *Ph* and gammacerane contents and an L-shaped distribution of C_{27}, C_{28}, and C_{29} steranes (Figure 16A–I). The *Pr*/*Ph* and gammacerane indices of the southern oil range from 1.04 to 1.07 (average of 1.06) and from 0.23 to 0.47 (average of 0.31), respectively (Table 3).

Siltstone Core Samples

Three oil-saturated siltstone core samples were collected from the Wei 18-5 well (Figure 15). The results show that all the samples featured low *Pr* and high *Ph* and gammacerane contents and an L-shaped distribution of C_{27}, C_{28}, and C_{29} steranes (Figure 15A–I). The *Pr*/*Ph* and gammacerane indices range from 0.20 to 0.35 (average of 0.28) and from 0.65 to 0.78 (average of 0.73), respectively.

DISCUSSION

Hydrocarbon Generation and Expulsion Potential

The hydrocarbon generation and expulsion potential of a source rock is determined by area, thickness, organic matter content, organic matter precursors, and thermal maturity (White and Gehman, 1979; Schmoker, 1994).

Paleogene shales were developed across the DD with a large area and thickness (Lu et al., 2013; Wang et al., 2015a; Zhang et al., 2017). Although the evaluation results of this large amount of data show that the organic matter content of shale is generally low, this is related to the fact that most of the shale samples obtained during the early exploration period are not source rocks.

Although studies have shown that regular steranes of some aquatic organisms such as brown algae are mainly C_{29}, and some oils from sub-Devonian deposits that lack terrestrial higher plant precursors are rich in C_{29} steranes (Moldowan et al., 1985; Fowler and Douglas, 1987), it is generally held that C_{27} and C_{28} steranes mainly originate from lower aquatic organisms, and C_{29} mainly stems from terrestrial higher plants (Huang and Meinschein, 1979). The relative abundance of C_{27}, C_{28}, and C_{29} regular steranes is a common index for revealing organic matter precursors. For the laminated shales, the C_{27}, C_{28}, and C_{29} distribution patterns exhibit L shapes in both the northern and southern regions, with the highest and lowest contents for C_{27} and C_{28}, respectively, indicating key sources of lower aquatic organisms (Figures 14A–D, F; 15F, I; 16R, U). For the northern massive shales, the distribution patterns of C_{27}, C_{28}, and C_{29} steranes are mainly reversed L and V shapes, with the highest content of C_{28} or C_{29} steranes (Figures 14E–G) and only a few L-shaped distributions (Figure 15R), indicating key sources were terrestrial higher plants. The C_{27}, C_{28}, and C_{29} distribution patterns of the southern massive shales are all reversed L and V shapes (Figures 14H, 16L, and 16O), indicating sources were predominantly terrestrial higher plants. Therefore, compared to the massive shales, sources of lower aquatic organisms are

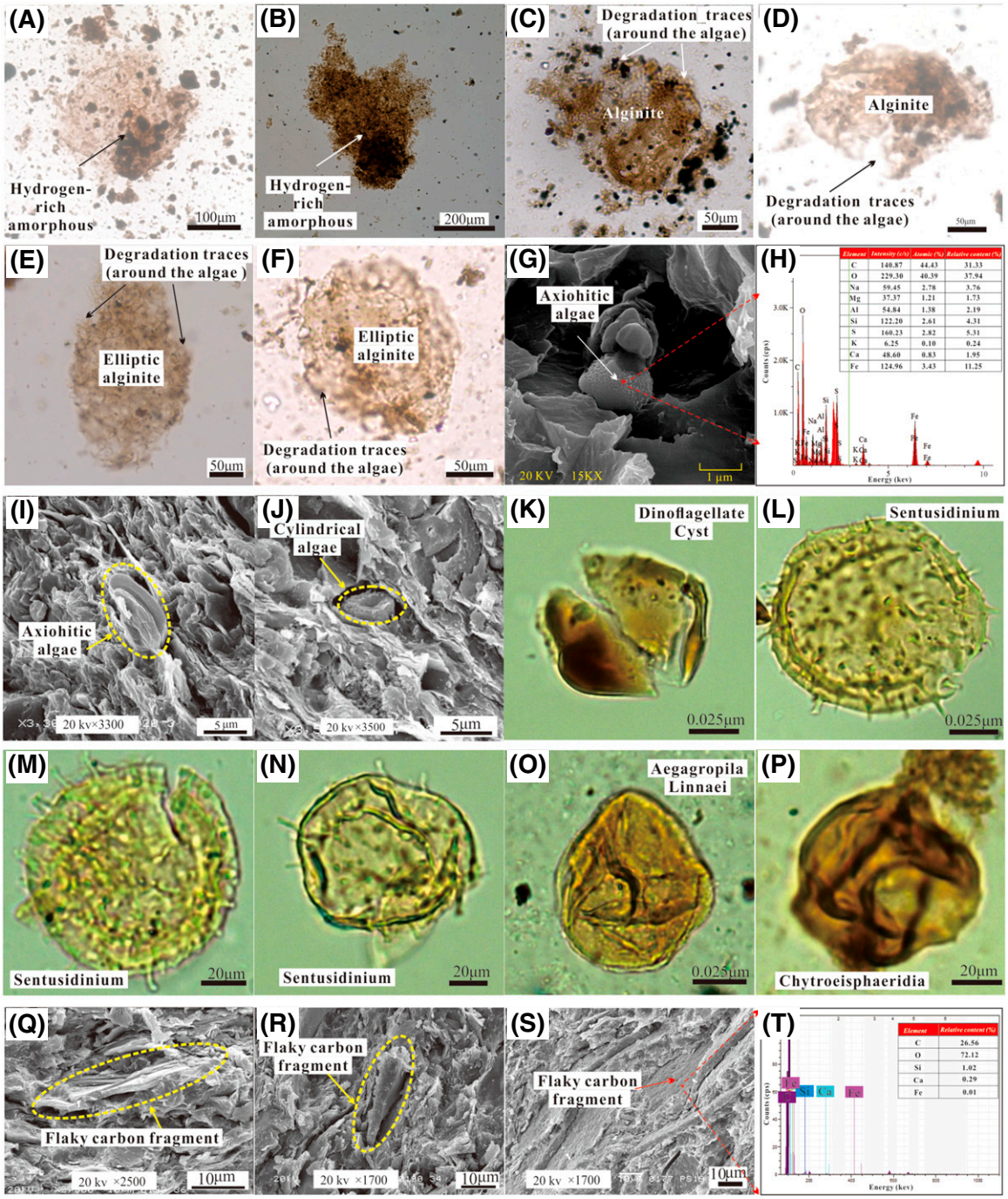

Figure 10. The optical microscopy, field emission scanning electron microscopy, and energy spectrum images showing the typical organic matter precursors of the Shahejie shales. (A) Well Ma 11-7, third member of the Shahejie Formation (E_2s_3); 3351.7 m, laminated shale; (B) well Wei 146, upper submember of fourth member of E_2s ($E_2s_4^U$), 2885.98 m, laminated shale; (C) well Pushen 18-8, upper submember of third member of E_2s ($E_2s_3^U$), 3191 m, laminated shale; (D) well Ma 11-7, E_2s_3, 3327.8 m, laminated shale; (E) well Ming 48, lower submember of third member of E_2s ($E_2s_3^L$), 2132.16 m, laminated shale; (F) well Pushen 18-1, $E_2s_3^U$, 3283.1 m, laminated shale; (G, H) well Pushen 18-8, $E_2s_3^U$, 3193 m, laminated shale; (I) well Qiancan 2, $E_2s_3^L$, 4271.4 m, laminated shale; (J) well Qiancan 2, $E_2s_3^L$, 4520.02 m, laminated shale; (K) well Ming 1, $E_2s_3^U$, 1710.1 m, laminated shale; (L) well Ming 36, $E_2s_3^U$, 1491 m, laminated shale; (M, N) well Wei 18-5, lower submember of first member of E_2s, 1801.48 m, laminated shale; (O) well Hu 5-52, $E_2s_3^L$, 2178.52 m, laminated shale; (P) well Wen 26, lower submember of second member of E_2s, 2965.12 m, laminated shale; (Q) well Tang 4, middle submember of third member of E_2s, 3708.9 m, massive shale; (R) well Pushen 8, $E_2s_4^U$, 4984.6 m, massive shale; (S, T) well Pushen 19, $E_2s_3^U$, 4350 m, massive shale.

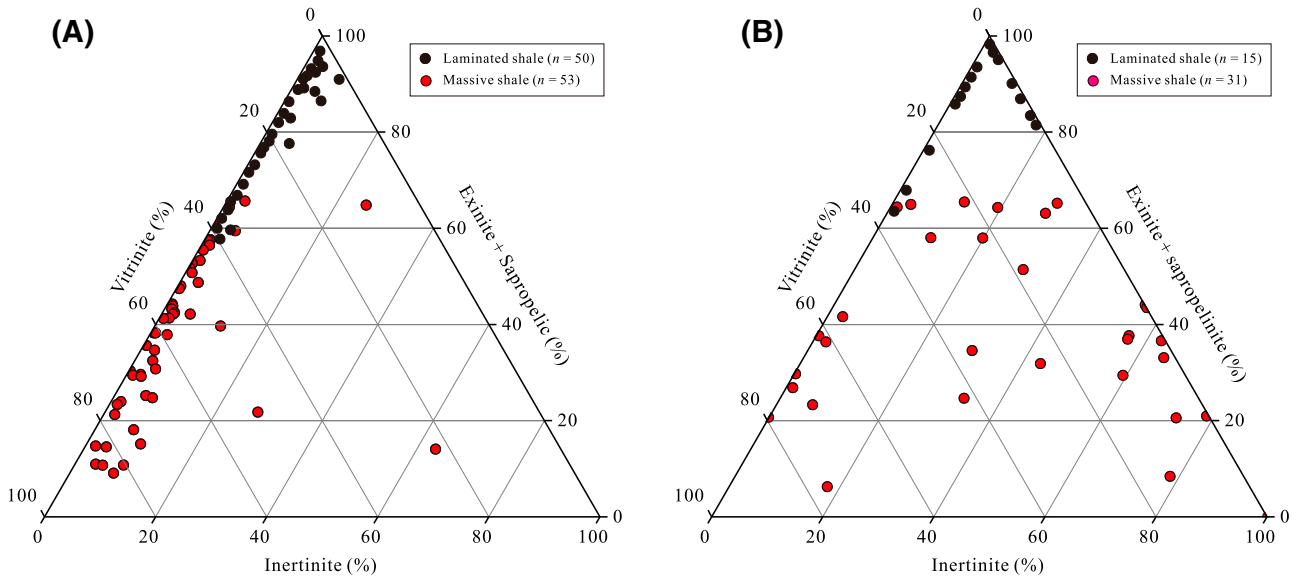

Figure 11. Kerogen maceral components of the Shahejie shales, showing kerogen within the massive shales is mainly composed of vitrinite and inertinite, whereas kerogen within the laminated shales is mainly composed of exinite and sapropelic. (A) Northern region; (B) southern region.

generally more abundant in the laminated shales. This is consistent with the results obtained by optical microscopy, FE-SEM, and energy spectrum analysis.

The northern and southern shales are within the peak-late mature stage (Figure 12). Further analysis shows that the R_o trends in the northern and southern regions are generally the same, but with slight differences. First, the depth of the southern shales entering the late mature or postmature stage is approximately 600 m deeper than that for the northern shales (Figure 12). This might be due to the different thermal histories and geothermal gradients between the northern and southern regions (Zuo et al., 2017). Second, the depth for the shales in Qiaokou-Baimijao entering the early and peak mature stages is less than that for the shales in the other areas, but the depth entering the late mature and postmature stages is the same or even larger than that in the other areas (Figure 12). This is likely related to the thick evaporites in Qiaokou-Baimijao, with a cumulative thickness of up to 950 m (Liu et al., 2014). Compared to shales and sandstones, evaporites feature a much higher thermal conductivity, resulting in a much easier heat transfer from deep to shallow strata, which leads to anomalously high temperature/geothermal gradients in the strata above the evaporites and anomalously low temperature/geothermal gradients in the strata beneath the evaporites (Liu and Jiang, 2013). This phenomenon is commonly observed in the Dongying depression (Li, 2005).

Compared with the massive shales, the *TOC* and *PG* values of the laminated shales are much higher, and the organic matter is much more oil prone within the mature stage. Therefore, the hydrocarbon generation potential of the laminated shales is qualitatively higher. This is mainly related to the differential redox and water salinity conditions between the laminated and massive shales during sedimentation. As described in Figures 14 and 15, the *Pr*/*Ph* and gammacerane indices indicate that both the northern laminated and massive shales were deposited in a reducing and brackish environment, whereas the reducing and water salinity degrees are much higher for the laminated shales. Moreover, the distributions of C_{27}, C_{28}, and C_{29} steranes indicate that the lower aquatic organism sources are more abundant than those in the massive shales. With increasing water salinity, the number of species and abundance of lower aquatic organisms first increase and then decrease because the resistance of aquatic organisms to lake salinity is limited, and only if the salinity exceeds the critical tolerance level of organisms will the species diversity and abundance sharply decrease

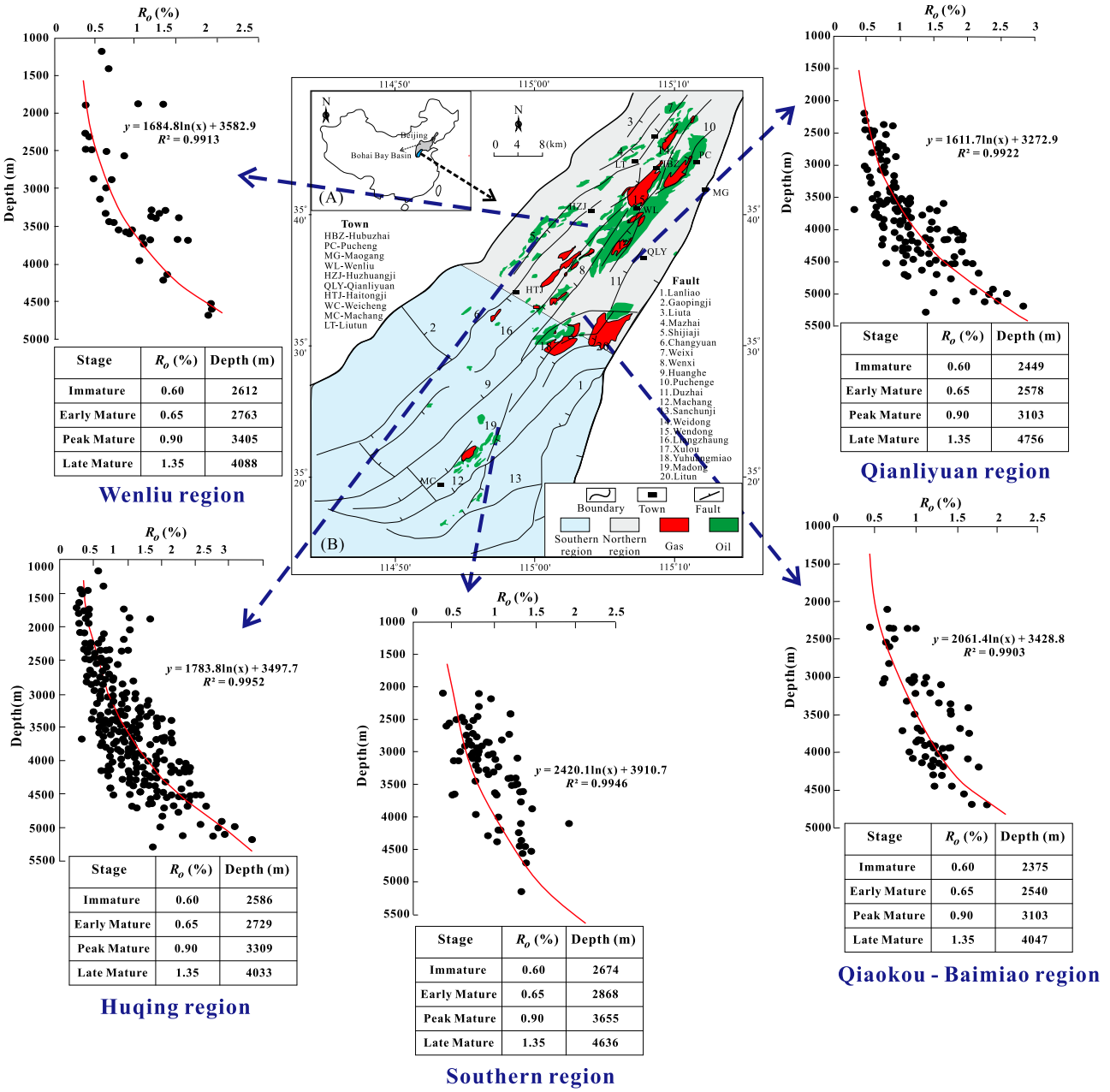

Figure 12. The vitrinite reflectance (R_o) versus depth of the Shahejie shales in different regions. R^2 = coefficient of determination.

(Kelts, 1988; Hite and Ander, 1991). Considering that the water body during Paleogene shale deposition in the DD was brackish, the number and abundance of lower aquatic organism species (paleoproductivity) increase with increasing salinity (Hu et al., 2018a). This phenomenon is also called algal blooming (Loftus and Greensmith, 1988), which is commonly seen in ancient lacustrine and marine deposits, such as the Kimmeridge Clay oil shales in England (Gallois, 1976) and Middle Old Red lacustrine sequences in the Orcadian Basin (Parnell, 1988). Algal blooms could consume most of the oxygen in the water and enhance the potential for water column anoxia. In addition, the increasing salinity would further result in water column stratification due to the density or salinity differences resulting from the dissolved salts (halocline) (Harrison and Digerfeldt, 1993), thus supporting the development of a reducing environment and, in turn, reinforcing the preservation conditions for organic matter (Kelts,

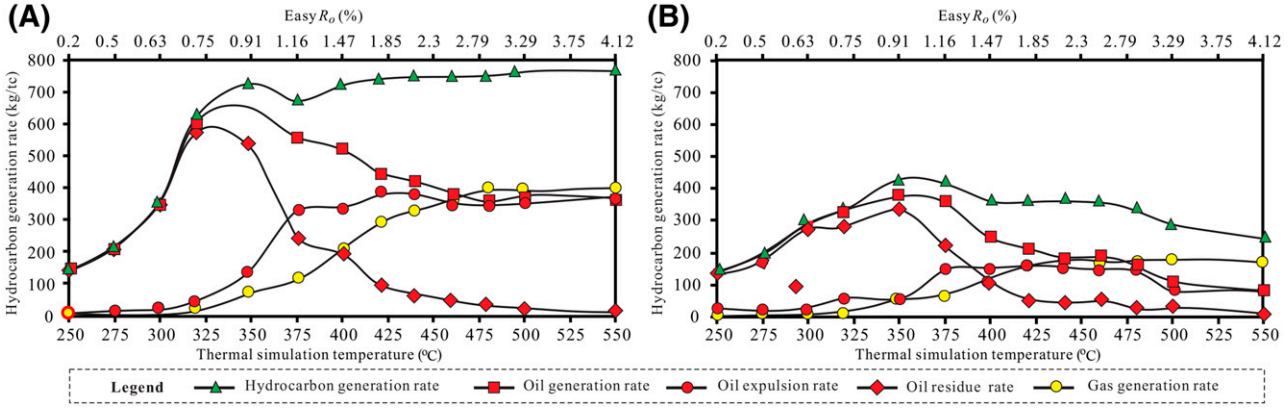

Figure 13. Thermal simulation experiments of two typical immature Shahejie shale core samples with different lithofacies. (A) Well Ming 8, middle submember of third member of Shahejie Formation ($E_2s_3^M$), 2024.8 m, laminated shale, total organic carbon (*TOC*) = 2.67 wt. %, maximum temperature (T_{max}) = 417°C, hydrogen index (*HI*) = 687 mg/g, type I kerogen; (B) well Hu 19-23, $E_2s_3^M$, 1735.38 m, massive shale, *TOC* = 4.27 wt. %, T_{max} = 427°C, *HI* = 553 mg/g, type II kerogen. Easy vitrinite reflectance (R_o) data for the pyrolysis experiments are simulated by the Vitrimat model (Sweeney and Burnham, 1990). kg/tc = kilograms per ton organic carbon.

1988; Hite and Ander, 1991). There were hardly any benthic organisms beneath the halocline (Jin, 2001). In addition, the Paleogene shales in the DD were deposited in a paleogeographic subtropical lake system, and therefore, seasonal lamina with abundant pyrite were easily developed in the stratified water body (Figure 4E, F).

Thermal simulation data were utilized to quantitatively compare the hydrocarbon generation and expulsion potentials between the laminated and massive shales. It is clear that, compared to the massive shales with approximately twice the *TOC* content, the hydrocarbon generation, oil generation, oil expulsion, and oil residue rates of the laminated shales are almost double those of the massive shales, and the gas generation rate is nearly three times as high. This is mainly related to the much higher hydrocarbon generation and expulsion capacities of the organic matter precursors in the laminated shales, which are mainly from lower aquatic organisms. In addition, in the saline lacustrine basins across the world, laminated shales are generally developed in association with evaporation (Katz, 1988; Horsfield et al., 1994; Zhang et al., 2017). Almost all the laminated shales

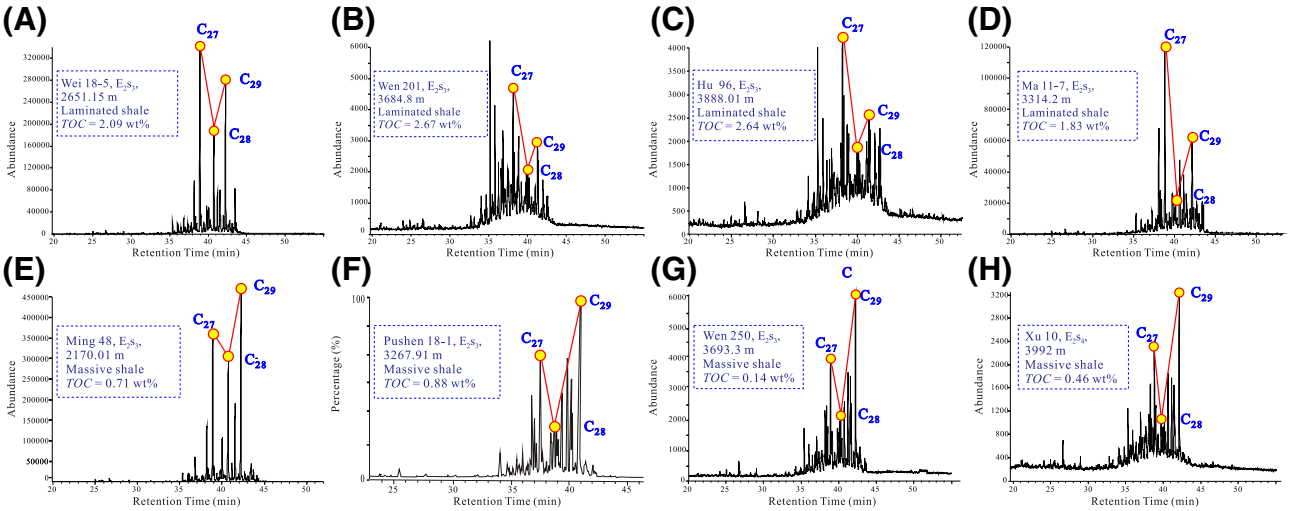

Figure 14. The relative abundance of ααα-C_{27}-20R (C_{27}), ααα-C_{28}-20R (C_{28}), and ααα-C_{29}-20R (C_{29}) regular steranes showing the typical organic matter precursors of the Shahejie shales. Northern shales: (A–C) and (E–G); southern shales: (D) and (H). E_2s_3 = third member of Shahejie Formation; E_2s_4 = fourth member of E_2s; *TOC* = total organic carbon.

Table 2. Total Organic Carbon and Biomarker Data for the 56 Paleogene Shale Core Samples in the Dongpu Depression, Bohai Bay Basin

Number	Well	Region	Stratum	Depth (m)	Lithology	*TOC* (wt. %)	*Pr*/*Ph*	Gammacerane Index
1	Wei 18-5	Northern	$E_2s_3^L$	2780.68	Laminated shale	4.45	0.30	0.49
2	Wei 18-5	Northern	$E_2s_3^M$	2660.95	Laminated shale	3.87	0.25	0.75
3	Wei 146	Northern	$E_2s_4^U$	2838.9	Laminated shale	3.29	0.49	1.47
4	Qiao 38-6	Northern	$E_2s_3^M$	3105.4	Laminated shale	2.92	0.29	0.63
5	Wen 13-54	Northern	$E_2s_3^M$	3241.0	Laminated shale	2.68	0.35	0.75
6	Wei 18-5	Northern	$E_2s_3^L$	2785.19	Laminated shale	2.67	0.45	0.49
7	Wen 15-14	Northern	$E_2s_3^U$	2376.5	Laminated shale	2.58	0.30	0.62
8	Wei 20	Northern	$E_2s_3^M$	2388.0	Laminated shale	2.41	0.26	0.91
9	Wen 201	Northern	$E_2s_3^L$	3679.65	Laminated shale	2.32	0.34	4.03
10	Pu 47	Northern	$E_2s_3^U$	3014.1	Laminated shale	2.25	0.32	1.45
11	Pu 115	Northern	$E_2s_3^U$	3090.89	Laminated shale	2.01	0.25	1.30
12	Pu 47	Northern	$E_2s_3^U$	3061.8	Laminated shale	2.00	0.43	0.98
13	Pu 115	Northern	$E_2s_3^U$	3131.5	Laminated shale	1.99	0.38	0.79
14	Wen 201	Northern	$E_2s_3^L$	3678.25	Laminated shale	1.39	0.39	2.10
15	Pushen 18-8	Northern	$E_2s_3^U$	3182.54	Laminated shale	1.20	0.36	0.63
16	Hu 83	Northern	$E_2s_3^U$	3828.0	Laminated shale	1.08	0.41	2.36
17	Wen 201	Northern	$E_2s_3^L$	3682.7	Laminated shale	1.06	0.59	1.59
18	Wen 250	Northern	$E_2s_3^L$	3674.5	Laminated shale	1.01	0.57	3.26
19	Pushen 18	Northern	$E_2s_3^M$	4236.59	Laminated shale	0.54	0.47	0.31
20	Hu 83	Northern	$E_2s_3^U$	3835.0	Laminated shale	0.31	0.43	1.87
21	Wen 201	Northern	$E_2s_3^L$	3684.8	Massive shale	2.63	0.52	2.09
22	Hu 19-23	Northern	$E_2s_3^M$	1736.44	Massive shale	2.10	0.37	0.27
23	Wen 250	Northern	$E_2s_3^L$	3680.6	Massive shale	1.26	0.62	1.63
24	Qing 67	Northern	$E_2s_1^L$	3047.7	Massive shale	1.14	0.21	1.69
25	Hu 83	Northern	$E_2s_3^U$	3804.5	Massive shale	0.78	0.42	0.34
26	Wen 223	Northern	$E_2s_3^U$	3212.6	Massive shale	0.77	0.71	0.10
27	Wen 201	Northern	$E_2s_3^L$	3686.3	Massive shale	0.65	0.94	0.29
28	Qiao 60	Northern	$E_2s_3^L$	4666.0	Massive shale	0.50	0.67	0.23
29	Wen 201	Northern	$E_2s_3^L$	3694.1	Massive shale	0.45	0.65	0.30
30	Qiao 60	Northern	$E_2s_3^L$	4665.5	Massive shale	0.39	0.59	0.34
31	Wen 201	Northern	$E_2s_3^L$	3699.7	Massive shale	0.35	0.63	0.51
32	Qiao 60	Northern	$E_2s_3^L$	4750.5	Massive shale	0.32	0.68	0.30
33	Hu 115	Northern	$E_2s_3^M$	3825.2	Massive shale	0.31	0.66	0.24
34	Qiao 60	Northern	$E_2s_3^L$	4737.3	Massive shale	0.28	0.54	0.34
35	Xinwen 195	Northern	$E_2s_3^L$	3705.5	Massive shale	0.26	0.64	0.15
36	Hu 83	Northern	$E_2s_3^M$	4262.7	Massive shale	0.23	0.49	0.57
37	Pushen 18	Northern	$E_2s_3^M$	4078.69	Massive shale	0.23	0.42	0.73
38	Qing 67	Northern	$E_2s_1^L$	2991.81	Massive shale	0.22	0.65	0.17
39	Pushen 18	Northern	$E_2s_3^M$	4074.89	Massive shale	0.21	0.41	0.57
40	Pushen 14	Northern	$E_2s_3^M$	3970.78	Massive shale	0.20	0.41	0.50
41	Pushen 13	Northern	$E_2s_3^M$	5090.88	Massive shale	0.16	0.24	0.65
42	Hu 83	Northern	$E_2s_3^U$	3748.8	Massive shale	0.16	0.57	0.81
43	Pushen 14	Northern	$E_2s_3^M$	3977.59	Massive shale	0.15	0.40	0.26
44	Hu 108	Northern	$E_2s_3^M$	4109.2	Massive shale	0.14	0.56	0.13
45	Wen 250	Northern	$E_2s_3^M$	3602.7	Massive shale	0.12	0.70	0.60
46	Wen 250	Northern	$E_2s_3^M$	3668.3	Massive shale	0.10	0.70	0.34
47	Hu 83	Northern	$E_2s_3^M$	4247.25	Massive shale	0.09	0.49	0.57
48	Xin 14	Southern	$E_2s_3^L$	4237.7	Massive shale	0.75	1.61	0.27

(*continued*)

Table 2. Continued

Number	Well	Region	Stratum	Depth (m)	Lithology	*TOC* (wt. %)	*Pr/Ph*	Gammacerane Index
49	Lin 1	Southern	$E_2s_1^L$	3650.21	Massive shale	0.33	0.52	0.51
50	Ma 11-7	Southern	$E_2s_3^L$	3314.2	Laminated shale	1.83	0.86	0.27
51	Pushen 6	Southern	$E_2s_3^M$	4649.2	Massive shale	0.22	0.51	0.25
52	Tang 8	Southern	$E_2s_3^L$	4368.89	Massive shale	0.20	0.45	0.32
53	Pushen 6	Southern	$E_2s_3^U$	4259.0	Massive shale	0.07	0.50	0.45
54	Qiao 35	Southern	$E_2s_3^M$	4055.5	Massive shale	0.76	0.44	0.31
55	Qiao 20	Southern	Es_3^M	3910.88	Massive shale	1.01	0.90	0.33
56	Bai 15	Southern	E_2s_3	3614.4	Laminated shale	1.37	1.76	0.15

Abbreviations: $E_2s_1^L$ = lower submember of first member of Shahejie Formation; $E_2s_1^U$ = upper submember of first member of E_2s; $E_2s_2^L$ = lower submember of second member of E_2s; $E_2s_2^U$ = upper submember of second member of E_2s; $E_2s_3^L$ = lower submember of third member of E_2s; $E_2s_3^M$ = middle submember of third member of E_2s; $E_2s_3^U$ = upper submember of third member of E_2s; $E_2s_4^L$ = lower submember of fourth member of E_2s; $E_2s_4^U$ = upper submember of fourth member of E_2s; *Pr/Ph* = pristane/phytane ratio; *TOC* = total organic matter.

with a high organic matter content are adjacent to or thinly interbedded with evaporites in the DD (Zhang et al., 2017; Xu et al., 2019). In particular, evaporite minerals have a notable catalytic impact on both hydrocarbon generation and pore space evolution in shales (Goldstein, 1983; Dembicki, 1992; Liu et al., 2016a), which accelerates hydrocarbon generation and expulsion. For the laminated shale samples, the simulation temperatures correspond to the oil generation peaks, and the oil residue rates are generally lower than those of the massive shale samples. This might be related to the generally lower activation energy of lower aquatic organisms than that of terrestrial higher plants (Ungerer, 1990; Jiang et al., 2005), which are the key components in laminated shales.

The results also show that for the laminated shale samples, the peak oil expulsion rate is more than twice that of the massive shale samples, and the oil expulsion efficiency (peak oil expulsion rate/peak oil generation rate) is 10% higher. In addition, for the laminated shale samples, the temperature corresponding to the simulated oil expulsion rate exceeding the oil residue rate is notably lower than that of the massive shale sample (Figure 13). This might have three causes. First, evaporite minerals accelerate the oil expulsion process by catalytically impacting oil generation and pore space evolution in shales (Goldstein, 1983; Dembicki, 1992; Liu et al., 2016b). Second, the laminated shales were mainly composed of lower aquatic organisms with a lower activation energy in terms of oil generation (Ungerer, 1990; Jiang et al., 2005). Third, extensive organic-rich and calcareous lamina were developed in the laminated shales (Figures 4D–F, 5A–C), and abundant fissures were generated between the lamina during diagenesis. In stark contrast to the extremely low lateral permeability of the massive shales, the lateral permeability along the lamina in the laminated shales is much higher, and hence, oil easily migrates along the abundant fissures. This could be further confirmed by the continuous and bright yellow fluorescence of the lamina (Figure 5A–C). Therefore, the hydrocarbon generation potential of the laminated shales is much higher than that of the massive shales and is more favorable for hydrocarbon expulsion.

Oil-Source Correlation

The biomarker *Pr/Ph*, gammacerane index, and relative abundances of C_{27}, C_{28}, and C_{29} regular steranes can be adopted to indicate the depositional environment and organic matter origin, which are commonly applied in oil-source correlation (Didyk et al., 1978; Powell and McKirdy, 1973; Huang and Meinschein, 1979). Generally, *Pr/Ph* lower than 1.0 and higher than 1.0 indicate reducing and oxidizing environments, respectively (Powell and McKirdy, 1973). Didyk et al. (1978) proposed that a *Pr/Ph* lower than 0.6 represents a hypersaline reducing environment. The gammacerane index is also an indicator of water stratification, which increases with increasing water salinity (Moldowan et al., 1985).

The *Pr/Ph* and gammacerane indices indicate that the northern laminated shales (*Pr/Ph*: 0.25–0.59 [average of 0.38]; gammacerane index: 0.31–4.03 [average of 1.34]) were deposited in a strongly

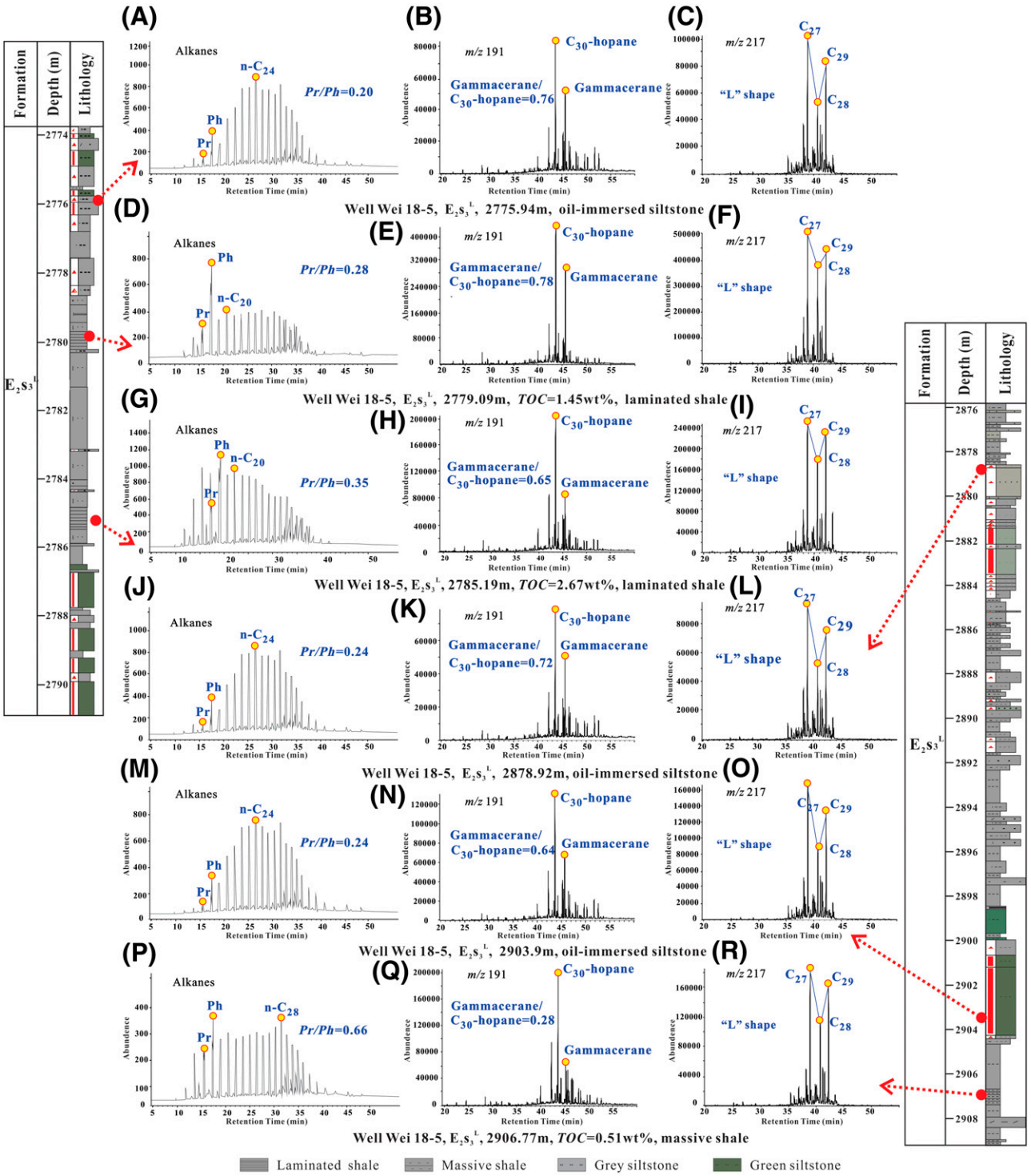

Figure 15. (A–R) Representative chromatograms of biomarkers identified in the northern Shahejie shales and oil from the well Wei 18-5. $E_2s_3^L$ = lower submember of the third member of Shahejie Formation; *m/z* = mass-to-charge ratio; *Pr/Ph* = pristane/phytane ratio; *TOC* = total organic carbon.

Table 3. Biomarker and Location Data for the 90 Paleogene Oil Samples in the Dongpu Depression, Bohai Bay Basin

Number	Profile	Well	Stratum	Depth (m)	*Pr*/*Ph*	Gammacerane Index
1	1	Ming 404c	$E_2s_2^L$	1615.0–1674.3	0.41	0.73
2	1	Ming 237c	$E_2s_3^L$	2155.0–2231.6	0.44	0.70
3	1	Ming 196c	$E_2s_2^L$	1664.6–1754.4	0.43	0.72
4	1	Ming 99	$E_2s_2^L$	1604.6–1875.0	0.44	0.73
5	1	Ming 63	$E_2s_3^U$	1796.3–1871.6	0.42	0.74
6	1	Wei 77-16	$E_2s_4^U$	2787.3–3012.6	0.43	0.74
7	1	Wei 22-53	$E_2s_3^L$	2712.1–2808.5	0.43	0.54
8	1	Wei 374	$E_2s_3^M$	3225.8–3304.8	0.59	0.40
9	1	Wei 360-65	$E_2s_3^U$	3009.6–3052.4	0.54	0.68
10	1	Wei 360-27	$E_2s_3^M$	3025.9–3099.0	0.62	0.72
11	1	Yun 9-3	$E_2s_3^U$	3132.0–3226.5	0.36	0.80
12	1	Pu 7-59	$E_2s_3^U$	3293.0–3644.6	0.47	0.59
13	1	Pu 138-7	$E_2s_3^M$	3868.1–4021.0	0.64	0.77
14	1	Pu 5-167	$E_2s_3^U$	3178.6–3251.5	0.39	0.71
15	1	Pu 6-155	$E_2s_3^M$	3176.0–3212.4	0.49	0.63
16	1	Pu 7-176	$E_2s_3^M$	3544.6–3643.9	0.52	0.68
17	1	Pu 1-103	$E_2s_2^U$	2448.6–2453.0	0.44	1.03
18	1	Pu 1-317	$E_2s_1^L$	2426.6–2437.5	0.45	0.73
19	2	Wei 95-c174	$E_2s_3^L$	1945.9–1981.0	0.40	0.56
20	2	Wei 95-199	$E_2s_3^L$	1879.8–1893.6	0.39	0.54
21	2	Wei 305-cc43	$E_2s_3^M$	2652.9–2745.6	0.31	0.37
22	2	Wei 305-53	$E_2s_3^M$	2784.9–2821.5	0.36	0.53
23	2	Wei 317-13	$E_2s_2^U$	2319.3–2348.3	0.44	0.73
24	2	Wei 355-2	$E_2s_3^U$	3273.6–3401.1	0.30	0.39
25	2	Wei 42-40	$E_2s_3^U$	3491.0–3726.9	0.54	0.51
26	2	Pu 138-6	$E_2s_2^U$	2403.0–2603.3	0.44	0.71
27	2	Pu 5-131	$E_2s_2^U$	2362.2–2573.3	0.44	0.73
28	2	Pu 4-1	$E_2s_3^U$	3039.3–3314.0	0.32	0.78
29	2	Pu 6-615	$E_2s_3^U$	3096.0–3298.6	0.48	0.67
30	2	Pu 6-165	$E_2s_2^U$	2557.5–3249.6	0.45	0.72
31	2	Puxin 119	$E_2s_3^U$	3063.3–3088.5	0.41	0.83
32	2	Pu 7-122	$E_2s_2^U$	2559.1–2580.4	0.63	0.74
33	2	Pu 6-577	$E_2s_2^L$	2750.7–2841.1	0.43	0.71
34	2	Pu 5-5723	$E_2s_2^U$	2420.2–2428.1	0.42	0.74
35	2	Pu 1-37	$E_2s_2^U$	2390.6–2399.0	0.40	0.81
36	3	Hu 19-65	$E_2s_3^M$	2132.9–2207.6	0.29	0.76
37	3	Hu 96-4	$E_2s_3^M$	3557.5–4214.6	0.50	1.92
38	3	Pushen 18-2	$E_2s_3^M$	4167–4207.3	0.54	1.12
39	3	Pushen 18	$E_2s_3^M$	3886.4–4237.1	0.53	0.82
40	3	Wen 142	$E_2s_2^L$	2449.1–3054.6	0.32	0.74
41	3	Wen 164	$E_2s_2^U$	1850–1907.8	0.42	0.96
42	3	Wen 38-45	$E_2s_3^M$	2675.4–2689.3	0.32	0.68
43	3	Wence 38-2	$E_2s_3^M$	2612.2–2739.6	0.34	0.62
44	3	Wence 38-6h	$E_2s_3^U$	1961.1–2016.4	0.46	0.69
45	3	Wen 38-84	$E_2s_3^U$	1967.6–2014.9	0.44	0.68
46	3	Wen 38-62	$E_2s_2^L$	2245.8–2481.5	0.44	0.69
47	3	Wenxin 38-15	$E_2s_2^L$	2355–2439.3	0.44	0.71
48	4	Hu 10-22	$E_2s_3^L$	2107.8–2497.9	0.47	0.54
49	4	Hu 10-10	$E_2s_3^U$	1776.2–1834	0.77	0.65
50	4	Hu 12-173	$E_2s_3^M$	2168.5–2202.4	0.50	0.53
51	4	Hu 39-20	$E_2s_2^U$	1748.5–1880.1	0.55	0.49

(*continued*)

Table 3. Continued

Number	Profile	Well	Stratum	Depth (m)	*Pr/Ph*	Gammacerane Index
52	4	Hu 12-158	$E_2s_3^M$	2214.1–2328.3	0.51	0.53
53	4	Hu 68-2	$E_2s_2^L$	2655.3–2797.5	0.46	0.63
54	4	Hu 63-20	$E_2s_2^U$	2782.4–2793.1	0.51	0.63
55	4	Hu 52-16	$E_2s_3^M$	2561.8–2594.3	0.49	0.70
56	4	Hu 52-22	$E_2s_3^L$	2936.5–3649.6	0.53	0.71
57	4	Wen 197	$E_2s_1^L$	2758.0–2777.3	0.16	1.21
58	4	Wence 194	$E_2s_2^L$	3287.8–3302.4	0.63	1.46
59	4	Wen 192	$E_2s_2^L$	3389.8-3647.0	0.63	1.76
60	4	Wen 188-9	$E_2s_2^L$	3343.8–3546.1	0.63	1.89
61	4	Wen 188-16	$E_2s_2^L$	3636.6–3952.9	0.61	1.50
62	4	Wen 79-60	$E_2s_2^L$	2856–3098	0.50	0.96
63	4	Wen 79-39	$E_2s_2^L$	2957.4–3040.8	0.54	0.73
64	4	Wen 138-c41	$E_2s_2^L$	3243.0–3424.6	0.55	0.97
65	4	Wen 138-42	$E_2s_2^L$	3206.8–3425.0	0.53	0.93
66	4	Wen 138-52	$E_2s_2^L$	3356.5–3454.4	0.57	0.93
67	4	Wen 138-27	$E_2s_2^L$	3480.9–3581.9	0.55	0.90
68	4	Wen 179-33	$E_2s_3^U$	3595.3–3904.6	0.51	0.73
69	4	Wen 79-172	$E_2s_2^L$	3167.3–3246.3	0.55	0.88
70	4	Wen 181-3	$E_2s_2^L$	3310.8–3884.9	0.64	0.73
71	5	Liu 17-4	$E_2s_1^L$	3315.3–3390.8	0.28	0.81
72	5	Liu 9-6	$E_2s_2^L$	3617.0–4301.8	0.77	1.85
73	5	Liu 24	$E_2s_2^U$	3197–3243.4	0.80	1.75
74	5	Liu 20	$E_2s_2^L$	3385.8–3608.4	0.70	2.63
75	5	Liu 31-3	$E_2s_2^L$	3498.3–3609.3	0.66	1.66
76	5	Qiao 29-17	$E_2s_2^L$	2557.5–2615.0	0.71	0.55
77	5	Qiao 29-16	$E_2s_2^L$	2394.2–2546.2	0.74	0.56
78	5	Qiaoce 29-4	$E_2s_2^L$	2504–2574.9	0.68	0.54
79	5	Qiao 29-6h	$E_2s_2^L$	2486.8–2582.4	0.69	0.54
80	5	Qiao 7-2	$E_2s_3^U$	2952.3–2993.4	0.79	0.69
81	5	Qiao 38-3	$E_2s_3^U$	3139.9–3242.8	0.87	0.56
82	5	Qiao 58-5	$E_2s_3^M$	3394.9–3581.8	0.71	0.50
83	6	Ma 26	$E_2s_3^U$	3229.4–3264.5	1.04	0.47
84	6	Ma 9-31	$E_2s_3^L$	2935.4–3208.9	1.04	0.40
85	6	Ma 11-4	$E_2s_3^M$	2968.1–3145.3	1.05	0.24
86	6	Ma 9-9	$E_2s_3^L$	3333.9–3363.6	1.07	0.23
87	6	Ma 11-89	$E_2s_3^L$	3216.1–3316.8	1.06	0.43
88	6	Chun 9-39	$E_2s_3^L$	3228.6–3575.5	1.07	0.25
89	6	Chun 9-45	$E_2s_3^L$	3291.6–3537.3	1.07	0.23
90	6	Ma 19-42	$E_2s_3^L$	2990.3–3103.5	1.05	0.23

Abbreviations: $E_2s_1^L$ = lower submember of first member of Shahejie Formation; $E_2s_1^U$ = upper submember of first member of E_2s; $E_2s_2^L$ = lower submember of second member of E_2s; $E_2s_2^U$ = upper submember of second member of E_2s; $E_2s_3^L$ = lower submember of third member of E_2s; $E_2s_3^M$ = middle submember of third member of E_2s; $E_2s_3^U$ = upper submember of third member of E_2s; $E_2s_4^L$ = lower submember of fourth member of E_2s; $E_2s_4^U$ = upper submember of fourth member of E_2s; *Pr/Ph* = pristane/phytane ratio.

reducing hypersaline environment. The northern massive shales (*Pr/Ph*: 0.21–0.94 [average of 0.55]; gammacerane index: 0.10-2.10 [average of 0.54]) were also developed in a reducing and brackish environment, but salinity oxygen depletion was less than those of the northern laminated shales. In assessing the C_{27}, C_{28}, and C_{29} sterane distributions, the organic matter of the northern laminated shales mainly originates from lower aquatic organisms, whereas that of the northern massive shales is derived from terrestrial higher plants. In the southern region, both the laminated and massive shales were

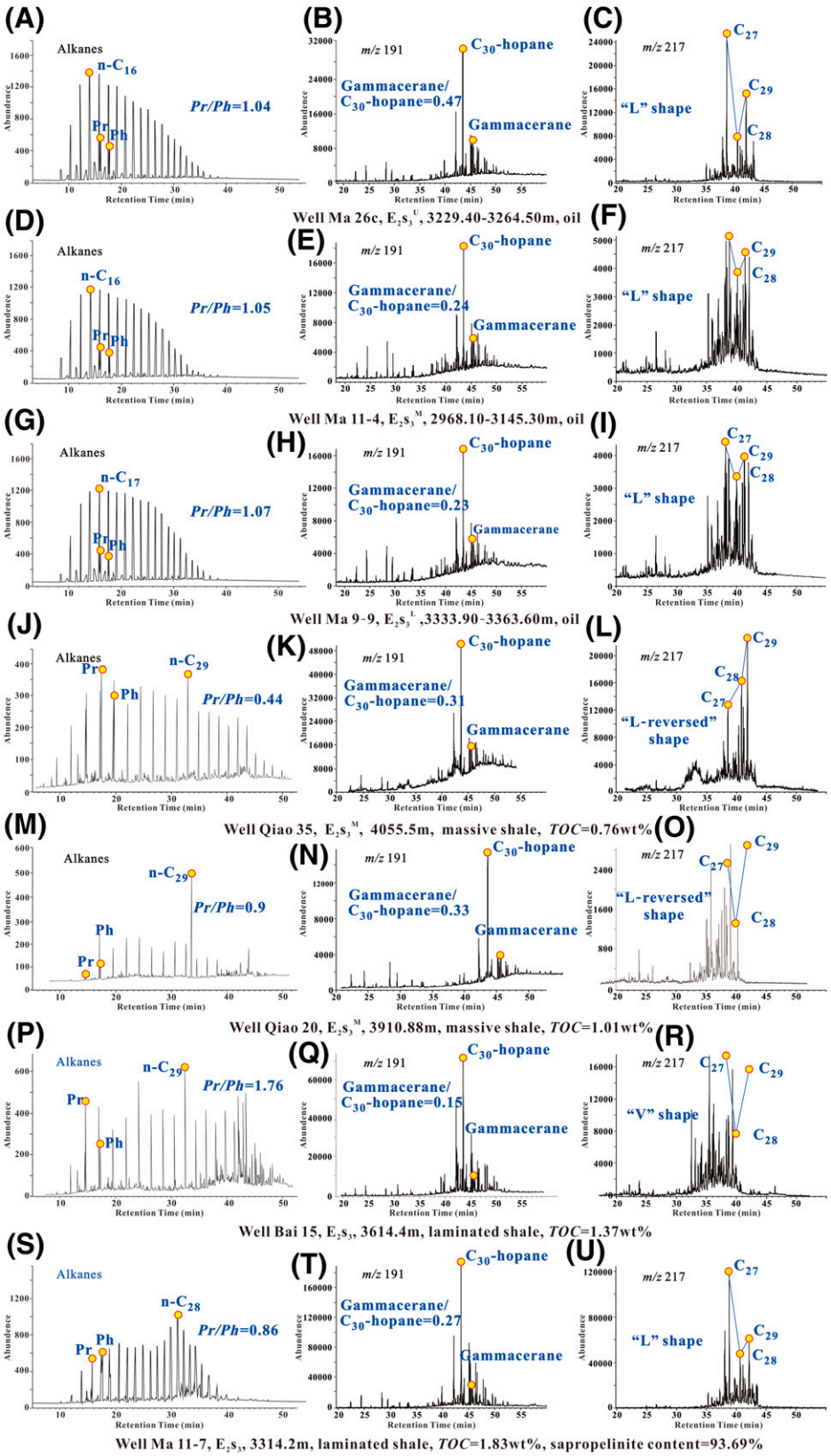

Figure 16. (A–U) Representative chromatograms of biomarkers identified in the southern Shahejie shales and oil from the Machang region. E_2s_3 = third member of Shahejie Formation; $E_2s_3^L$ = lower submember of third member of E_2s; $E_2s_3^M$ = middle submember of third member of E_2s; $E_2s_3^U$ = upper submember of third member of E_2s; *m/z* = mass-to-charge ratio; *Pr/Ph* = pristane/phytane ratio; *TOC* = total organic carbon.

deposited in a freshwater depositional environment, with a low level of oxygenation or reduction conditions (*Pr/Ph*: 0.44–1.76 [average of 0.84]; gammacerane index: 0.15–0.51 [average of 0.32]). In comparison, the abundance of lower aquatic organisms in the laminated shales is much larger than that in the organic matter of the massive shales.

The analytical results indicate that the *Pr/Ph* and gammacerane indices of almost all the northern laminated shale samples occur in the range of less than 0.7 and greater than 0.5 (blue rectangle with the dotted lines, Figure 17A), respectively, whereas the *Pr/Ph* and gammacerane indices of a few northern massive shales occur in the range of less than 0.7 and greater than 0.5 (blue rectangle with the dotted lines, Figure 17A). For the *Pr/Ph* and gammacerane indices of the southern laminated and massive shales, none were less than 0.7 or greater than 0.5 (Figure 17A). No clear correlation was observed in analyzing the *TOC*, *Pr/Ph*, and gammacerane index (Figure 17B, C). However, the *Pr/Ph* of good source rocks (shales with *TOC* contents higher than 1 wt. %) were generally less than 0.7, which is mainly due to the good preservation conditions in a reducing environment (Didyk et al., 1978; Tang et al., 2020). In addition, the gammacerane index of good source rocks is commonly greater than 0.5, which is mainly related to the good preservation conditions in stratified water environments and algal blooming in water with a relatively high salinity (Hite and Ander, 1991; Hu et al., 2018a). Therefore, for the Paleogene shales in the DD, almost all the shales with *TOC* contents greater than 1 wt. % have a *Pr/Ph* lower than 0.7 and a gammacerane index higher than 0.5.

For the oil samples, the *Pr/Ph* and gammacerane indices indicate that the northern oil (profiles 1–5 in Figure 1B) (*Pr/Ph*: 0.16–0.87 [average of 0.51]; gammacerane index: 0.37–2.63 [average of 0.83]) were sourced from shales deposited in a strong reducing

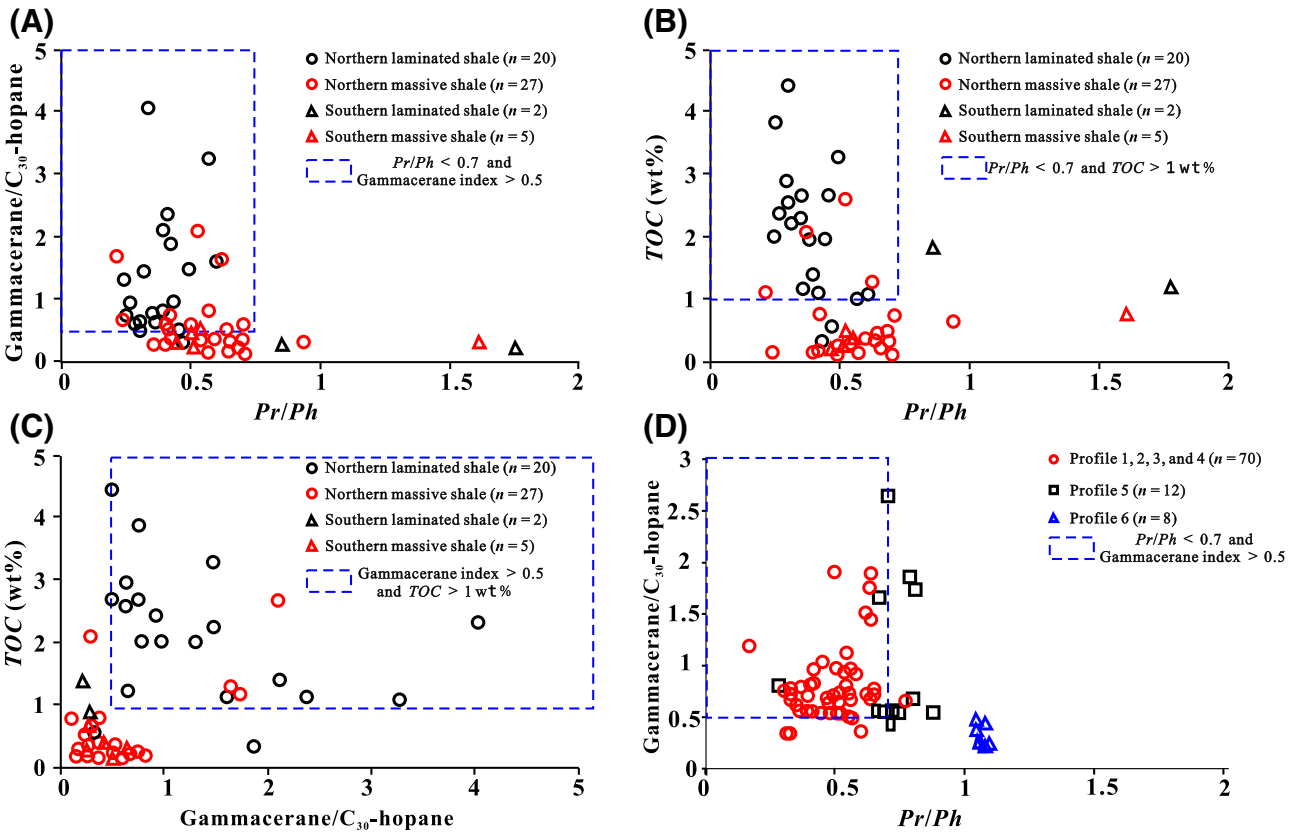

Figure 17. Correlation between (A) Pristane/phytane ratio (*Pr/Ph*) and gammacerane index (gammacerane/C_{30}-hopane), (B) *Pr/Ph* and total organic carbon (*TOC*), and (C) gammacerane index and *TOC* of the Shahejie shales, and (D) *Pr/Ph* and gammacerane index of the 90 oil samples from the Shahejie strata.

and hypersaline environment, whereas the southern oil (profile 6 in Figure 1B) (*Pr/Ph*: 1.04–1.07 [average of 1.06]; gammacerane index: 0.23-0.47 [average of 0.31]) was sourced from shales deposited in a weak oxidizing-weak reducing and freshwater environment. In analyzing the C_{27}, C_{28}, and C_{29} sterane distributions, the organic matter in all the oil samples originated from lower aquatic organisms.

Further analysis indicates that almost all the northern oils have a *Pr/Ph* less than 0.7 and a gammacerane index greater than 0.5 (blue rectangle with the dotted lines, Figure 17D), suggesting a high consistency with the biomarker characteristics of the northern laminated shales with *TOC* contents greater than 1 wt. % (Figure 17A–C). Therefore, the effective source rocks in the northern region should be mainly laminated shales with *TOC* contents greater than 1 wt. %. Regarding the biomarker indices of the southern oils, none of which occur in the blue rectangle with the dotted lines (Figure 17D), the distributions of C_{27}, C_{28}, and C_{29} steranes for the southern oils are all L shaped (Figure 16C, F, and I, respectively), also indicating a high consistency with the biomarker characteristics of the southern laminated shales (Figures 14D; 16R, and U, respectively). Therefore, the hydrocarbon generation potential analysis and oil-source correlation both indicate that the hydrocarbons are mainly sourced from the laminated shales.

For the oil-saturated siltstone core samples from northern well Wei 18-5, the *Pr/Ph* and gammacerane index indicate that the oil (*Pr/Ph*: 0.20–0.35 [average of 0.28]; gammacerane index: 0.65–0.78 [average of 0.73]) was sourced from shales deposited in a strong reducing and hypersaline environment. In analyzing the L-shaped distributions of C_{27}, C_{28}, and C_{29} steranes, all the oil was sourced from shales with abundant lower aquatic organisms. Vertically, the biomarker indices of the oil-immersed siltstone sample at a depth of 2775.94 m (Figure 15A–C) are highly consistent with those of the adjacent laminated shale samples at depths of 2779.09 and 2785.19 m (Figure 15D–I). In addition, the biomarker indices of the oil--saturated siltstone sample at depths of 2878.92 and 2903.9 m (Figure 15J–O) are similar to those of the oil-saturated siltstone sample at a depth of 2775.94 m (Figure 15A–C) and are also highly consistent with those of the laminated shale samples at depths of 2779.09 and 2785.19 m (Figure 15D–I) but are greatly different from those of the massive shale sample at a depth of 2906.77 m (Figure 15P–R). Therefore, the oil within the siltstone cores from the Wei 18-5 well was sourced from the northern laminated shales.

Extremely thick shales were found over nearly 40 yr of petroleum exploration in the southern region, most of which are massive shales (Wu et al., 2003; Wang et al., 2015a). Almost all the previous studies considered these thick massive shales as key source rocks, but the oil-source correlation analysis results between the oil and massive shales does not support this (He et al., 2010; Bian et al., 2017). Recently, source rock reevaluation studies were conducted, and it was found that thin, laminated shales were developed and interbedded with the thick, massive shales, such as in well Ma 11-7. Further analysis reveals that the *TOC* content of these laminated shales is generally high, with abundant sapropelinites (nearly 93.7%) in the kerogen, indicating high hydrocarbon generation and expulsion potentials (Figure 16P–U). Moreover, analysis of the biomarker indices shows that the oil and laminated and massive shales, all display *Pr/Ph* and gammacerane indices that are generally high and low, respectively, showing no notable difference among the oil and laminated and massive shale samples (Figure 16). However, in view of the distributions of C_{27}, C_{28}, and C_{29} steranes, the oil samples exhibit a high consistency with the biomarker characteristics of the southern laminated shales (Figure 16). Therefore, similar to the northern region, the laminated shales are also key source rocks in the southern region.

Implications for Petroleum Exploration in Lacustrine Basins

Combined with the forward and inverse analyses, the laminated shales with *TOC* contents higher than 1 wt. % were determined as the primary source rocks in the DD. In retrospect, the consideration of the extremely thick massive shales as key source rocks was based largely on two reasons. First, over the 40 yr of petroleum exploration in the DD, the early source rock evaluation studies were concentrated on the shale intervals adjacent to the oil-immersed reservoirs. These shales are generally poor in organic matter and lack oil-prone organic matter precursors but are extensively distributed and very thick. The

hydrocarbon generation amounts of these thick shales are very large based on the volumetric method for resource evaluation (Duan et al., 2008; Li and Jiang, 2009; Liu and Jiang, 2013). Actually, the hydrocarbon expulsion efficiency of thick shales is commonly low but is generally great for thin shales. For example, absolute expulsion efficiency for thin shales with thickness less than 2 m can be up to 80%–90% (Mackenzie et al., 1983; Leythaeuser et al., 1984). Whereas for shales with thickness of 28 m, the expulsion efficiency of shales from the middle section to the boundary is 27% (Leythaeuser et al., 1987, 1988), and the expulsion efficiency of the shales with thickness of 40 m is only 3% on average (Chen et al., 2014). Second, influenced by the assumption that laminated shales have a low hydrocarbon expulsion potential due to high residual oil content (Zhang, 2005), some researchers did not consider them as key source rocks, although some laminated shales with oil shows were sporadically encountered in core descriptions during well drilling. Guided by this biased viewpoint, serious problems emerged in the petroleum resource evaluation of lacustrine basins. The gross thickness, distribution area, and average *TOC* content are three key parameters in hydrocarbon generation quantity evaluations of source rocks. By considering the extensive and extremely thick massive shales as key source rocks, their gross thickness and distribution area were greatly exaggerated, while the average *TOC* content was reduced by the thick massive shales with dispersed organic matter, which was extremely inflated by these massive shales (organic-lean shales), masking the actual contribution of laminated shales (organic-rich shales). Coincidentally, similar situations have been seen in marine hydrocarbon systems. For example, 93% of the proven hydrocarbon in the Gulf of Mexico Basin originates from the Upper Jurassic Tithonian marine marl-dominated shales, with high *TOC* contents of 2–22.8 wt. % and limited thickness of 30–170 m (Guzmán-Vega et al., 2001). Therefore, the focus of studies should be reoriented to laminated shales in petroleum exploration in lacustrine basins.

Extensive and extremely thick lacustrine shales have developed across the world. Both laminated and massive shales are composed of particles smaller than 0.0039 mm, with a particle content higher than 50% (Macquaker and Adams, 2003), but notable differences exist in the mineral composition, organic matter occurrence, texture, formation conditions, and distribution between laminated and massive shales. Laminated shales are the key source rocks for conventional petroleum resources and the main targets for shale oil resources, whereas massive shales mainly function as cap rocks (Liu et al., 2018b). These differences result in different degrees of geologic importance for petroleum generation, migration, accumulation, and enrichment. For the extensive, extremely thick, and heterogeneous lacustrine shales, specific division of the laminated and massive shales and comparative studies are vital for petroleum exploration in lacustrine basins.

CONCLUSIONS

The Paleogene shales in the DD consist of laminated and massive shales. Compared to the massive shales, the *TOC* and *PG* values of the laminated shales are much greater and the organic matter precursors are much more oil prone, but the thickness is relatively small. Thermal simulation analysis shows that the hydrocarbon generation and expulsion potentials of the laminated shales are much higher than those of the massive shales.

The northern laminated and massive shales were deposited in reducing and brackish environments, but the reducing and salinity conditions during laminated shale deposition were much higher. The organic matter precursors in the northern laminated shales mainly originate from lower aquatic organisms, whereas those in the northern massive shales are derived from terrestrial higher plants. The southern laminated and massive shales were both deposited in a freshwater depositional environment, with low oxidizing or reducing conditions, and the lower aquatic organism sources in the laminated shales are more abundant than those in the massive shales. The northern oil and oil-saturated samples are characterized by low *Pr* and high *Ph* and gammacerane contents, while southern oil and oil-saturated samples are characterized by high *Pr* and low *Ph* and gammacerane contents. The northern oil originated from shales deposited in a strong reducing and saline environment, and the southern oil originated from shales deposited in a weak oxidizing-weak reducing and freshwater environment.

Combined with the forward and inverse analyses, the laminated shales with *TOC* contents higher than 1 wt. % were identified as the primary source rocks. The focus of studies should be reoriented to laminated shales in further petroleum exploration in saline lacustrine basins.

REFERENCES CITED

Bian, L. B., G. D. Liu, M. L. Sun, J. D. Li, Z. C. Niu, and D. L. Yang, 2017, Geochemical characteristics of source rocks and oil-source correlation of Shahejie Formation in Fangliji area, Dongpu sag, China [in Chinese with English abstract]: China Offshore Oil and Gas, v. 29, no. 6, p. 53–60, doi:10.11935/j.issn.1673-1506.2017.06.006.

Bird, K. J., 1994, Ellesmerian(!) petroleum system, North Slope, Alaska, USA, *in* L. B. Magoon and W. G. Dow, eds., The petroleum system—From source to trap: AAPG Memoir 60, p. 339–358.

Burgess, J. D., 1974, Microscopic examination of kerogens (dispersed organic matter) in petroleum exploration: Geological Society of America Bulletin, v. 153, p. 19–30, doi:10.1130/SPE153-p19.

Calvert, S. E., R. M. Bustin, and E. D. Ingall, 1996, Influence of water column anoxia and sediment supply on the burial and preservation of organic carbon in marine shales: Geochimica et Cosmochimica Acta, v. 60, no. 9, p. 1577–1593, doi:10.1016/0016-7037(96)00041-5.

Cao, J., R. F. Yang, G. Hu, W. X. Hu, S. P. Yao, X. M. Xie, Y. Q. Gao, and J. Gao, 2018, Hydrocarbon potential of the Lower Cretaceous mudstones in coastal southeastern China: AAPG Bulletin, v. 102, no. 2, p. 333–366, doi:10.1306/0503171617917074.

Chen, J. P., Y. G. Sun, N. N. Zhong, Z. K. Huang, C. P. Deng, L. J. Xie, and H. Han, 2014, The efficiency and model of petroleum expulsion from the lacustrine source rocks within geological frame [in Chinese with English abstract]: Acta Geologica Sinica, v. 88, no. 11, p. 2005–2032.

Chen, Z. H., W. Huang, Q. Liu, L. Y. Zhan, and S. C. Zhang, 2016, Geochemical characteristics of the Paleogene shales in the Dongying depression, eastern China: Marine and Petroleum Geology, v. 73, p. 249–270, doi:10.1016/j.marpetgeo.2016.02.022.

Dembicki, J. H., 1992, The effects of the mineral matrix on the determination of kinetic parameters using modified Rock Eval pyrolysis: Organic Geochemistry, v. 18, no. 4, p. 531–539, doi:10.1016/0146-6380(92)90116-F.

Deng, Y. H., and T. Sun, 2019, Discussion on the symbiotic relationship between high quality source rocks and large oilfields: China Offshore Oil and Gas, v. 31, p. 1–8, doi:10.11935/j.issn.1673-1506.2019.05.001.

Didyk, B. M., B. R. T. Simoneit, S. C. Brassell, and G. Eglinton, 1978, Organic geochemical indicators of palaeoenvironmental conditions of sedimentation: Nature, v. 272, no. 5650, p. 216–222, doi:10.1038/272216a0.

Duan, H. M., P. Gao, X. W. Wang, and J. J. Zhang, 2008, The secondary hydrocarbon generation of the Shahejie source rocks in the Dongpu Depression [in Chinese with English abstract]: Journal of Oil and Gas Technology, v. 30, no. 1, p. 206–209.

Fowler, M. G., and A. G. Douglas, 1987, Saturated hydrocarbon biomarkers in oils of Late Precambrian age from Eastern Siberia: Organic Geochemistry, v. 11, no. 3, p. 201–213, doi:10.1016/0146-6380(87)90023-4.

Gallois, R. W., 1976, Coccolith blooms in the Kimmeridge Clay and origin of North Sea oil: Nature, v. 259, no. 5543, p. 473–475, doi:10.1038/259473b0.

Goldstein, T. P., 1983, Geocatalytic reactions in formation and maturation of petroleum: AAPG Bulletin, v. 67, p. 152–159, doi:10.1306/03B5ACD7-16D1-11D7-8645000102C1865D.

Guzmán-Vega, M. A., L. C. Ortíz, J. R. Román-Ramos, L. M. Morales, L. C. Valdéz, E. Vázquez-Covarrubias, and G. Ziga-Rodríguez, 2001, Classification and origin of petroleum in the Mexican Gulf Coast Basin: An overview, *in* C. Bartolini, R. T. Buffler, and A. Cantú-Chapa, eds., The western Gulf of Mexico Basin: Tectonics, sedimentary basins and petroleum systems: AAPG Memoir 75, p. 127–142.

Hakimi, M. H., W. H. Abdullaha, and M. R. Shalaby, 2012, Madbi-Biyadh/Qishn (!) petroleum system in the onshore Masila Basin of the Eastern Yemen: Marine and Petroleum Geology, v. 35, no. 1, p. 116–127, doi:10.1016/j.marpetgeo.2012.01.009.

Halbouty, M. T., 1980, Methods used, and experience gained in exploration for new oil and gas in highly explored (mature) areas: AAPG Bulletin, v. 64, no. 8, p. 1210–1222, doi:10.1306/2F919463-16CE-11D7-8645000102C1865D.

Harrison, S. P., and G. Digerfeldt, 1993, European lake as palaeohydrological and palaeo-climatic indicators: Quaternary Science Reviews, v. 12, no. 4, p. 233–248, doi:10.1016/0277-3791(93)90079-2.

He, F., G. X. Jing, and L. H. Wei, 2010, Research significance of good source rocks in Dongpu depression [in Chinese with English abstract]: Journal of Oil and Gas Technology, v. 32, no. 4, p. 185–188.

Hite, R. J., and D. E. Ander, 1991, Petroleum and evaporites, *in* J. Melvin, ed., Evaporites, petroleum and mineral resources: Amsterdam, Elsevier, p. 349–411

Horsfield, B., D. J. Curry, and K. Bohacs, 1994, Organic geochemistry of freshwater and alkaline lacustrine sediments in the Green River Formation of the Washakie Basin, Wyoming, USA: Organic Geochemistry, v. 22, no. 3-5, p. 415–440, doi:10.1016/0146-6380(94)90117-1.

Hu, T., X. Q. Pang, F. J. Jiang, Q. F. Wang, X. H. Liu, Z. Wang, S. Jiang, et al., 2021, Movable oil content evaluation of lacustrine organic-rich shales: Methods and a novel quantitative evaluation model: Earth-Science Reviews, v. 214, 103545, 26 p., doi:10.1016/j.earscirev.2021.103545.

Hu, T., X. Q. Pang, S. Jiang, Q. F. Wang, T. W. Xu, K. Lu, C. Huang, Y. Y. Chen, and X. W. Zheng, 2018a, Impact of paleosalinity, dilution, redox, and paleoproductivity on

organic matter enrichment in a saline lacustrine rift basin: A case study of Paleogene organic-rich shale in Dongpu depression, Bohai Bay Basin, eastern China: Energy & Fuels, v. 32, no. 4, p. 5045–5061, doi:10.1021/acs.energyfuels.8b00643.

Hu, T., X. Q. Pang, S. Jiang, Q. F. Wang, X. W. Zheng, X. J. Ding, Y. Zhao, C. X. Zhu, and H. Li, 2018b, Oil content evaluation of lacustrine organic-rich shale with strong heterogeneity: A case study of the Middle Permian Lucaogou Formation in Jimusaer Sag, Junggar Basin, NW China: Fuel, v. 221, p. 196–205, doi:10.1016/j.fuel.2018.02.082.

Hu, T., X. Q. Pang, S. Yu, X. L. Wang, H. Pang, J. G. Guo, F. J. Jiang, W. B. Shen, Q. F. Wang, and J. Xu, 2016, Hydrocarbon generation and expulsion characteristics of Lower Permian P1f source rocks in the Fengcheng area, northwest margin, Junggar Basin, NW China: implications for tight oil accumulation potential assessment: Geological Journal, v. 51, no. 6, p. 880–900, doi:10.1002/gj.2705.

Huang, F., and M. A. Xin, 1995, Geochemical evaluation methods for terrestrial source rocks: (SY/T 5735-1995): The oil and gas industry standard of the People's Republic of China: Beijing, Petroleum Industry Press, 19 p.

Huang, W. Y., and W. G. Meinschein, 1979, Sterols as ecological indicators: Geochimica et Cosmochimica Acta, v. 43, no. 5, p. 739–745, doi:10.1016/0016-7037(79)90257-6.

Ji, Y. L., and J. H. Feng, 2003, Lowstand delta sedimentary of Paleogene in Dongpu Sag: Petroleum Exploration and Development, v. 30, no. 1, p. 112–114, doi:10.3321/j.issn:1000-0747.2003.01.034.

Jiang, F. J., X. Q. Pang, J. Bai, X. H. Zhou, J. Li, and Y. H. Guo, 2016, Comprehensive assessment of source rocks in the Bohai Sea area, eastern China: AAPG Bulletin, v. 100, no. 6, p. 969–1002, doi:10.1306/02101613092.

Jiang, H., X. Q. Pang, H. S. Shi, Q. H. Yu, Z. Cao, R. Yu, D. Chen, Z. L. Long, and F. J. Jiang, 2015, Source rock characteristics and hydrocarbon expulsion potential of the Middle Eocene Wenchang formation in the Huizhou depression, Pearl River Mouth basin, South China Sea: Marine and Petroleum Geology, v. 67, p. 635–652, doi:10.1016/j.marpetgeo.2015.06.010.

Jiang, Q. G., Q. Wang, Q. Q. Cheng, C. M. Zhang, and W. B. Liu, 2005, Discussion on the characteristics of hydrocarbon generation of different maceral source rocks: Petroleum Exploration and Development, v. 27, p. 521–518, doi:10.3969/j.issn.1001-6112.2005.05.015.

Jin, Q., 2001, Importance and research about effective hydrocarbon source rocks [in Chinese with English abstract]: Petroleum Geology & Recovery Efficiency, v. 8, p. 1–4, doi:10.3969/j.issn.1009-9603.2001.01.

Jin, Q., M. Zha, and L. Zhao, 2001, Identification of effective source rocks in the Tertiary evaporate facies in the Western Qaidam Basin [in Chinese with English abstract]: Acta Sedimentologica Sinica, v. 19, p. 125–129, doi: 10.3969/j.issn.1000-0550.2001.01.021.

Katz, B. J., 1988, Clastic and carbonate lacustrine systems: an organic geochemical comparison (Green River Formation and East African lake sediments): Geological Society, London, Special Publications 1988, v. 40, p. 81–90, doi:10.1144/GSL.SP.1988.040.01.08.

Katz, B. J., 1995, Factors controlling the development of lacustrine petroleum source rocks—An update, *in* A. Y. Huc, ed., Paleogeography, paleoclimate, and source rocks, AAPG Studies in Geology 40, p. 61–79, doi:10.1306/St40595C3.

Katz, B. J., and G. M. Kahle, 1988, Basin evaluation: A supply-side approach to resource assessment: Indonesian Petroleum Association, v. 1, p. 135–168, doi:10.29118/IPA.2260.135.168.

Kelts, K., 1988, Environments of deposition of lacustrine petroleum source rocks: An introduction: Geological Society, London, Special Publications 1988, v. 40, p. 3–26, doi:10.1144/GSL.SP.1988.040.01.02.

Lazar, O. R., K. M. Bohacs, and J. H. Macquaker, 2015, Capturing key attributes of fine-grained sedimentary rocks in outcrops, cores, and thin sections: Nomenclature and description guidelines: Journal of Sedimentary Research, v. 85, no. 3, p. 230–246, doi:10.2110/jsr.2015.11.

Lewan, M. D., and J. A. Williams, 1987, Evaluation of petroleum generation from resinite by hydrous pyrolysis: AAPG Bulletin, v. 71, no. 2, p. 207–214, doi:10.1306/94886D71-1704-11D7-8645000102C1865D.

Leythaeuser, D., A. Mackenzie, R. G. Schaefer, and M. Bjorøy, 1984, A novel approach for recognition and quantification of hydrocarbon migration effects in shale-sandstone sequences: AAPG Bulletin, v. 68, no. 2, p. 196–219, doi:10.1306/AD4609FE-16F7-11D7-8645000102C1865D.

Leythaeuser, D., M. Radke, and H. Willsch, 1988, Geochemical effects of primary migration of petroleum in Kimmeridge source rocks from Brae field area, North Sea. II: Molecular composition of alkylated naphthalenes, phenanthrenes, benzo- and dibenzothsiophenes: Geochimica et Cosmochimica Acta, v. 52, no. 12, p. 2879–2891, doi:10.1016/0016-7037(88)90155-X.

Leythaeuser, D., R. G. Schaefer, and M. Radke, 1987, On the primary migration of petroleum: 12th World Petroleum Congress, Houston, Texas, April 26–May 1, 1987, p. 227–236.

Li, D. L., Q. M. Shi, N. Z. Mi, and Y. Xu, 2020, The type, origin and preservation of organic matter of the fine-grain sediments in Triassic Yanhe Profile, Ordos Basin, and their relation to paleoenvironment condition: Journal of Petroleum Science Engineering, v. 188, 106875, 14 p., doi:10.1016/j.petrol.2019.106875.

Li, F. J., 2005, The development of the secondary pore of underlying formation in Dongying depression and analysis of its affecting factors [in Chinese with English abstract]: Journal of Chongqing University of Science and Technology (Natural Sciences Edition), v. 7, no. 4, p. 9–12, doi:10.3969/j.issn.1673-1980.2005.04.003.

Li, X. Y., and Y. L. Jiang, 2009, Characteristics and estimation of Es3 salty lacustrine facies source rocks in Puwei sag, Dongpu depression [in Chinese with English abstract]: Petroleum Geology and Recovery Efficiency, v. 16, p. 12–16, doi:10.3969/j.issn.1009-9603.2009.02.004.

Liang, D. G., 1998, Effective source rock evaluation in the Slope Belt in Manjiaer Depression, Tarim Basin [in Chinese with English abstract]: The 7th National Organic Geochemistry Conference in China, Xiamen City, China, December 1–7, 1998, p. 37–38.

Liu, B., J. X. Shi, X. F. Fu, Y. F. Lv, X. D. Sun, L. Gong, and Y. F. Bai, 2018a, Petrological characteristics and shale oil enrichment of lacustrine fine-grained sedimentary system: A case study of organic-rich shale in first member of Cretaceous Qingshankou Formation in Gulong Sag, Songliao Basin, NE China: Petroleum Exploration and Development, v. 45, no. 5, p. 884–894, doi:10.1016/S1876-3804(18)30091-0.

Liu, C. L., H. Li, and X. Zhang, 2016a, Geochemical characteristics of the Paleogene and Neogene saline lacustrine source rocks in the western Qaidam Basin, northwestern China: Energy & Fuels, v. 30, no. 6, p. 4537–4549, doi:10.1021/acs.energyfuels.6b00269.

Liu, G. H., Z. L. Huang, F. R. Chen, and Z. X. Jiang, 2016b, Reservoir characterization of Chang 7 member shale: A case study of lacustrine shale in the Yanchang Formation, Ordos Basin, China: Journal of Natural Gas Science and Engineering, v. 34, p. 458–471, doi:10.1016/j.jngse.2016.06.071.

Liu, J. D., and Y. L. Jiang, 2013, Thermal evolution characteristics of Paleogene source rocks and their main controlling factors in northern part of Dongpu Depression [in Chinese with English abstract]: Geology China, v. 40, no. 2, p. 498–507, doi:10.3969/j.issn.1000-3657.2013.02.014.

Liu, J. D., Y. L. Jiang, Y. M. Tan, X. S. Mu, 2014, Relationship between gypsum-salt rock and oil-gas in Dongpu Depression of Bohai Gulf Basin [in Chinese with English abstract]: Acta Sedimentologica Sinica, v. 32, no. 1, p. 126–137, doi:10.14027/j.cnki.cjxb.2014.01.015.

Liu, Q., X. J. Yuan, S. H. Lin, H. Guo, and D. W. Cheng, 2018b, Depositional environment and characteristic comparison between lacustrine mudstone and shale: A case study from the Chang 7 Member of the Yanchang Formation, Ordos Basin [in Chinese with English abstract]: Oil & Gas Geology, v. 39, no. 3, p. 531–540, doi: 10.11743/ogg20180310.

Loftus, G. W. F., and J. T. Greensmith, 1988, The lacustrine Burdiehouse Limestone Formation–a key to the deposition of the Dinantian oil shales of Scotland, *in* A. J. Fleet, K. Kelts, and M. R. Talbot, eds., Lacustrine petroleum source rocks: Geological Society, London, Special Publications 1988, v. 40, p. 219–234., 10.1144/GSL.SP.1988.040.01.19.

Loucks, R. G., R. M. Reed, S. C. Ruppel, and D. M. Jarvie, 2009, Morphology, genesis, and distribution of nanometer-scale pores in siliceous mudstones of the Mississippian Barnett Shale: Journal of Sedimentary Research, v. 79, no. 12, p. 848–861, doi:10.2110/jsr.2009.092.

Lu, K., Y. H. Zuo, B. Mei, H. M. Cao, and Y. H. Ding, 2013, Paleo-sedimentary environments of the Dongpu depression and their impact on organic matter abundance [in Chinese with English abstract]: Geology & Exploration, v. 49, no. 3, p. 589–594.

Mackenzie, A. S., D. Leythaeuser, R. G. Schaefer, and M. Bjorøy, 1983, Expulsion of petroleum hydrocarbons from shale source rocks: Nature, v. 301, no. 5900, p. 506–509, doi:10.1038/301506a0.

Macquaker, J. H. S., and A. E. Adams, 2003, Maximizing information from fine-grained sedimentary rocks: an inclusive nomenclature for mudstones: Journal of Sedimentary Research, v. 73, no. 5, p. 735–744, doi:10.1306/012203730735.

Magoon, L. B., and K. J. Bird, 1985, Alaskan North Slope petroleum geochemistry for the Shublik Formation, Kingak Shale, Pebble Shale Unit, and Torok Formation: *in* L. B. Magoon and G. E. Claypool, eds., Alaska North Slope oil/source rock correlation study: AAPG Studies in Geology 20, p. 31–48, doi:10.1306/St20445C2.

Mello, M. R., W. U. Mohriak, A. M. Koutsoukos, and J. C. A. Figueira, 1991, Brazilian and West African oils: Generation, migration, accumulation and correlation: 13th World Petroleum Congress, Buenos Aires, Argentina, October 20–25, 1991, v. 2, p. 153–164.

Moldowan, J. M., W. K. Seifert, and E. J. Gallegos, 1985, Relationship between petroleum composition and depositional environment of petroleum source rocks: AAPG Bulletin, v. 69, no. 8, p. 1255–1268, doi:10.1306/AD462BC8-16F7-11D7-8645000102C1865D.

Momper, A., 1978, Oil migration limitations suggested by geological and geochemical considerations, *in* W. H. Roberts and R. J. Cordell, eds., Physical and chemical constraints on petroleum migration, AAPG Continuing Education Course Note Series, v. 8, p. B1–B60, doi:10.1306/CE8396C2.

Pang, X. Q., 1995, Theory and application of the hydrocarbon expulsion threshold [in Chinese]: Beijing, Petroleum Industry Press, 248 p.

Pang, X. Q., Z. M. Chen, and F. J. Chen, 1993, Petroleum-bearing basin geologic history, thermal history, generation, residual and hydrocarbon-expulsion history quantitative model and hydrocarbon source rocks quantitative evaluation [in Chinese with English abstract]: Beijing, Geological Publishing House, 160 p.

Pang, X. Q., M. W. Li, S. M. Li, and Z. J. Jin, 2005, Geochemistry of petroleum systems in the Niuzhuang South Slope of Bohai Bay Basin: Part 3. Estimating hydrocarbon expulsion from the Shahejie formation: Organic Geochemistry, v. 36, no. 4, p. 497–510, doi:10.1016/j.orggeochem.2004.12.001.

Parnell, J., 1988, Lacustrine petroleum source rocks in the Dinantian Oil Shale Group, Scotland: A review, *in* A. J. Fleet, K. Kelts, and M. R. Talbot, eds., Lacustrine petroleum source rocks: Geological Society, London, Special Publications 1988, v. 40, p. 235–246, doi:10.1144/GSL.SP.1988.040.01.20.

Peng, J. W., X. Q. Pang, H. S. Shi, H. J. Peng, and S. Xiao, 2016, Hydrocarbon generation and expulsion characteristics of Eocene source rocks in the Huilu area, northern Pearl River Mouth Basin, South China Sea: Implications for tight oil potential: Marine and Petroleum Geology, v. 72, p. 463–487, doi:10.1016/j.marpetgeo.2016.02.006.

Peters, K. E., and M. R. Cassa, 1994, Applied source rock geochemistry, *in* L. B. Magoon and W. G. Dow, eds., The petroleum system—From source to trap: AAPG Memoir 60, p. 93–120, doi:10.1306/M60585.

Peters, K. E., L. B. Magoon, K. J. Bird, Z. C. Valin, and M. A. Keller, 2006, North Slope, Alaska: Source rock distribution, richness, thermal maturity, and petroleum charge: AAPG Bulletin, v. 90, no. 2, p. 261–292, doi:10.1306/09210505095.

Peters, K. E., R. L. Scott, J. E. Zumberge, Z. C. Valin, and K. J. Bird, 2008, De-convoluting mixed crude oil in Prudhoe Bay Field, North Slope, Alaska: Organic Geochemistry, v. 39, no. 6, p. 623–645, doi:10.1016/j.orggeochem.2008.03.001.

Powell, T. G., and D. M. McKirdy, 1973, Relationship between ratio of pristane to phytane, crude oil composition and geological environment in Australia: Nature, v. 243, no. 124, p. 37–39, doi:10.1038/physci243037a0.

Rahman, M., and R. R. F. Kinghorn, 1995, A practical classification of kerogens related to hydrocarbon generation: Journal of Petroleum Geology, v. 18, no. 1, p. 91–102, doi:10.1111/j.1747-5457.1995.tb00743.x.

Saikia, M. M., and T. K. Dutta, 1980, Depositional environments of source beds of high-wax oils in Assam Basin, India: AAPG Bulletin, v. 64, no. 3, p. 427–430, doi:10.1306/2F91899B-16CE-11D7-8645000102C1865D.

Schmoker, J. W., 1994, Volumetric calculation of hydrocarbons generated, *in* L. B. Magoon and W. G. Dow, eds., The petroleum system—From source to trap: AAPG Memoir 60, p. 323–326, doi:10.1306/M60585.

Su, H., L. P. Qu, and J. C. Zhang, 2006, Tectonic evolution and extensional pattern of rifted basin: A case study of Dongpu depression [in Chinese with English abstract]: Oil & Gas Geology, v. 27, no. 1, p. 70–77, doi:10.3321/j.issn:0253-9985.2006.01.012.

Sweeney, J. J., and A. K. Burnham, 1990, Evaluation of a simple model of vitrinite reflectance based on chemical kinetics: AAPG Bulletin, v. 74, no. 10, p. 1559–1570, doi:10.1306/0C9B251F-1710-11D7-8645000102C1865D.

Tang, L., Y. Song, X. Q. Pang, Z. X. Jiang, Y. C. Guo, H. G. Zhang, Z. H. Pan, and H. Jiang, 2020, Effects of paleo sedimentary environment in saline lacustrine basin on organic matter accumulation and preservation: A case study from the Dongpu Depression, Bohai Bay Basin, China: Journal of Petroleum Science Engineering, v. 185, 106669, 19 p., doi:10.1016/j.petrol.2019.106669.

Taylor, G. H., M. Teichmüller, A. Davis, C. F. K. Diessel, R. Littke, and P. Robert, 1998, Organic petrology: Berlin, Gebrüder Borntraeger, 704 p.

Tian, J. Q., F. Hao, X. H. Zhou, and H. Y. Zou, 2017, Distribution, controlling factors, and oil-source correlation of biodegraded oils in the Bohai offshore area, Bohai Bay basin, China: AAPG Bulletin, v. 101, no. 3, p. 361–386, doi:10.1306/07251614105.

Ungerer, P., 1990, State of the art of research in kinetic modelling of oil formation and expulsion: Organic Geochemistry, v. 16, no. 1-3, p. 1–25, doi:10.1016/0146-6380(90)90022-R.

Wang, M., N. Sherwood, Z. S. Li, S. F. Lu, W. G. Wang, A. H. Huang, J. Peng, and K. Lu, 2015a, Shale oil occurring between salt intervals in the Dongpu Depression, Bohai Bay Basin, China: International Journal of Coal Geology, v. 152, p. 100–112, doi:10.1016/j.coal.2015.07.004.

Wang, M., R. W. T. Wilkins, G. Q. Song, L. Y. Zhang, X. Y. Xu, Z. Li, and G. H. Chen, 2015b, Geochemical and geological characteristics of the $Es3^L$ lacustrine shale in the Bonan sag, Bohai Bay Basin, China: International Journal of Coal Geology, v. 138, p. 16–29, doi:10.1016/j.coal.2014.12.007.

Wang, M., Z. Q. Guo, C. X. Jiao, S. F. Lu, J. B. Li, H. T. Xue, J. J. Li, J. Q. Li, and G. H. Chen, 2019, Exploration progress and geochemical features of lacustrine shale oils in China: Journal of Petroleum Science Engineering, v. 178, p. 975–986, doi:10.1016/j.petrol.2019.04.029.

Wang, Y., K. E. Peters, J. M. Moldowan, K. J. Bird, and L. B. Magoon, 2014, Cracking, mixing, and geochemical correlation of crude oils, North Slope, Alaska. AAPG Bulletin, v. 98, no. 6, p. 1235–1267, doi:10.1306/01081412197.

White, D. A., and H. M. Gehman, 1979, Methods of estimating oil and gas resources: AAPG Bulletin, v. 63, p. 2183–2192, doi:10.1306/2F918900-16CE-11D7-8645000102C1865D.

Wicks, J. L., M. L. Buckingham, and J. H. Dupree, 1991, Endicott field–U.S.A., North Slope basin, Alaska, *in* N. H. Foster and E. A. Beaumont, eds., Structural traps V: AAPG treatise of petroleum geology: Atlas of oil and gas fields, p. 1–25.

Wu, G. X., Z. P. Wang, J. B. Sun, and S. J. Wang, 2003, Problem discussion on evaluation of continental source rocks [in Chinese with English abstract]: Fault-block Oil and Gas Field, v. 10, p. 28–31, doi:10.3969/j.issn.1005-8907.2003.03.009.

Xu, T. W., H. A. Zhang, J. D. Li, and W. Zhao, 2019, Characters of hydrocarbon generation and accumulation of salt-lake facies in Dongpu Sag, Bohai Bay Basin [in Chinese with English abstract]: Oil and Gas Geology, v. 40, no. 2, p. 248–261, doi:10.11743/ogg20190204.

Yurchenko, I. A., J. M. Moldowan, and K. E. Peters, 2018, The role of calcareous and shaly source rocks in the composition of petroleum expelled from the Triassic Shublik Formation, Alaska North Slope: Organic Geochemistry, v. 122, p. 52–67, doi:10.1016/j.orggeochem.2018.04.010.

Zhang, H. A., T. W. Xu, and Y. X. Zhang, 2017, Development characteristics and significance of high quality source rocks of salty lake in Dongpu Depression [in Chinese with English abstract]: Fault-block Oil and Gas Field, v. 24, p. 437–441, doi:10.6056/dkyqt201704001.

Zhang, L. Y., 2005, A restudy on the hydrocarbon occurrence of "enriched organic matter": A case study of Dongying Depression [in Chinese with English abstract]: Geochimica, v. 34, no. 6, p. 619–625, doi:10.19700/j.0379-1726.2005.06.009.

Zheng, L. Y., J. Z. Qin, S. He, G. Y. Li, and Z. M. Li, 2009, Preliminary study of formation porosity thermocompression

simulation experiment of hydrocarbon generation and expulsion [in Chinese with English abstract]: Petroleum Geology and Experiment, v. 31, no. 3, p. 296–302, doi:10.3969/j.issn.1001-6112.2009.03.017.

Zhu, G. Y., and Q. Jin, 2003, Geochemical characteristics of two sets of excellent source rocks in Dongying Depression [in Chinese with English abstract]: Acta Sedimentologica Sinica: v. 21, no. 3, p. 506–512, doi:10.3969/j.issn.1000-0550.2003.03.022.

Zou, C. N., R. K. Zhu, Z. Q. Chen, G. O. James, S. T. Wu, D. Z. Dong, Z. Qiu, et al., 2019, Organic-matter-rich shales of China: Earth-Science Reviews, v. 189, p. 51–78, doi:10.1016/j.earscirev.2018.12.002.

Zuo, Y. H., B. Ye, W. T. Wu, Y. X. Zhang, W. X. Ma, S. L. Tang, and Y. S. Zhou, 2017, Present temperature field and Cenozoic thermal history in the Dongpu depression, Bohai Bay Basin, North China: Marine and Petroleum Geology, v. 88, p. 696–711, doi:10.1016/j.marpetgeo.2017.08.037.